

Contents lists available at ScienceDirect

# Journal of the Mechanics and Physics of Solids

journal homepage: www.elsevier.com/locate/jmps





# Stress discontinuity and singularity around the vertex of a triangular inhomogeneity

Chunlin Wu a,b, Huiming Yin b,\*

- <sup>a</sup> Shanghai Institute of Applied Mathematics and Mechanics, School of Mechanics and Engineering Science, Shanghai University, No. 99 Shangda Road, Shanghai, 200044, China
- <sup>b</sup> Department of Civil Engineering and Engineering Mechanics, Columbia University, 610 Seeley W. Mudd 500 West 120th Street, NY, 10027, United States

## ARTICLE INFO

#### Keywords: Stress singularity Asymptotic stress analysis Equivalent inclusion method Airy's stress function Green's function

## ABSTRACT

The stress field around a vertex of angular inhomogeneity has been investigated by Eshelby's equivalent inclusion method (EIM). Different from Eshelby's problem for ellipsoidal inhomogeneity with a uniform or polynomial eigenstrain, a singular eigenstrain field is derived by Airy's stress function and asymptotic analysis, in which the singular elastic fields can be expressed in terms of the distance to the vertex. The discontinuity of Eshelby's tensor along the boundary has been analytically derived and are used in the stress equivalence condition at the vertex, which can be converted into an eigenvalue problem with the integral of the Green's function and singular eigenstrain over the inhomogeneity. To verify the solution, when the opening angle  $2\beta$  at the vertex approaches zero, the triangular void reduces to a slit-like crack, and the paper reproduces the classic solution of  $1/\sqrt{r}$  singularity. When  $\beta$  increases from 0 to  $\pi/2$ , the singularity parameter  $\lambda$  around the vertex of the triangular void reduces at different pace under the symmetric and antisymmetric loading conditions. When a triangular inhomogeneity exhibits nonzero stiffness and different angles,  $\lambda$  changes with the stiffness ratio,  $\beta$ , and loading conditions, and the dominant stress singularity around the vertex and stress discontinuity across the boundary are analytically provided. Particularly, the stress singularity for an adhesive interface with varying stiffness provides insight for structure repair and integration.

## 1. Introduction

Stress singularity has been a fascinating and attractive topic in solid mechanics. The discussion of strong singular behavior can be traced back to the nineteenth century, the infinite elastic fundamental solution (Thomson (Lord Kelvin), 1848), namely Kelvin's solution. Subsequently, the fundamental solutions have been extended to surface loads on the half-space (Boussinesq, 1885), and concentrate force within the semi-domain Mindlin (1936), which exhibit a strong stress singularity  $r^{-2}$  and  $r^{-1}$  for three-dimensional (3D) and two-dimensional (2D) problems (Wang, 1985), respectively. In addition to concentrated loads, material discontinuities (Bogy, 1968), geometric features (Williams, 1952; Dempsey and Sinclair, 1979) and loading aspects (Dundurs and Markenscoff, 1989) also induce stress singularities. It is challenging to evaluate the local field directly in numerical methods due to the computational convergence and stability. Surface integral in 3D (Eshelby, 1951) and contour integral in 2D (Eshelby, 1956; Rice, 1968) have often been used to quantify the singularity. The analytical solution of singularity provides a straightforward and robust approach to directly show the local field in the neighborhood of the singularity.

E-mail addresses: chunlinwu@shu.edu.cn (C. Wu), yin@civil.columbia.edu (H. Yin).

<sup>\*</sup> Corresponding author.

In the literature, there are several schools of analytical methods to identify singularity. Williams (1952) utilized Airy's stress function and separation of variables to investigate stress singularities of single-material wedge problems. Subsequently, Dempsey and Sinclair (1979) extended William's method by taking derivatives with respect to the singularity parameter  $\lambda$ , which can identify logarithmic singularities for the composite wedge. A similar approach using complex potentials can solve the single-material wedge problem (Williams, 1956; Muskhelishvili, 2010) with a compact notation. Bogy (1968) applied the Mellin transform to study singularities caused by the material mismatch. In addition, Eshelby's equivalent inclusion method (EIM) can transfer an ellipsoidal inhomogeneity problem into fracture analysis by changing the aspect ratio of the ellipsoid (semi-axis  $a_1, a_2, a_3$ ). For example, setting  $a_1 = a, a_2 \rightarrow 0, a_3 \rightarrow \infty$ , one can solve the classic slit-like crack problem (Giordano and Colombo, 2007; Zhou et al., 2013). Since Eshelby's tensor of ellipsoidal is constant for interior observing points, the eigenstrain of the slit-like crack problem is also constant if given a uniform far-field load, and the exterior fields exhibit  $1/\sqrt{r}$  singularity through limiting Eshelby's tensor. This method can also be extended to other crack problems, such as penny-shaped cracks, and the solution scheme can be changed with Griffith's criteria as well (Mura, 1987).

Extending Eshelby's solutions on other geometric shapes, Rodin (1996) obtained Eshelby's tensor for polygonal or polyhedral inclusion with a uniform eigenstrain. Sevostianov and Kachanov (2007) investigated the effective elastic properties of ellipsoids and compared them with the non-ellipsoidal cases. Moreover, Zhou et al. (2014) investigated the necessity of applying semi-analytical solution schemes for cases of multiple and complex-shaped inclusions. Ma and Korsunsky (2014) provided the formulation in integral form for inhomogeneity problems with an arbitrary shape, but the eigenstrain distribution in an angular inhomogeneity was not studied.

Sun et al. (2012) and Yue et al. (2015) studied the full-space anisotropic piezoelectric inclusion problem. By virtue of the Green's function and equivalent body force transformation, the authors converted domain integrals into boundary integrals, composed of elementary closed-form expression. Chiang (2015) considers inclusion problems in orthotropic media. The author derived a more compact Green's function and conducted an integral over line segment under traction, and the author revealed logarithmic singularity around two ends. Furthermore, this work (Chiang, 2015) explored more results in specific inclusions under dilatational eigenstrain, such as polygon-approximated circles. Recently, Trotta's group (Trotta et al., 2016, 2017) commented on Rodin's integral scheme (Rodin, 1996) that using the transformation coordinate may not be straightforward. Hence, they proposed an integral scheme dependent on the Cartesian coordinate, simplifying the trivial process of domain integrals over polygons and polyhedrons. Due to the challenge of representing the local varying eigenstrain using a constant term, Wu and Yin (2021) derived Eshelby's tensors with polynomial eigenstrain containing uniform, linear, quadratic and even higher order terms. Although such a scheme can provide reasonable predictions for ellipsoidal or elliptical inhomogeneities, it seldom considers the singular distribution of eigenstrain and stress fields around vertices.

Subsequently, Wu et al. (2021) proposes a domain discretization method on polyhedral inhomogeneities, which assigns eigenstrain on nodes of sub-elements, but the analytical rigor is lost by given a finite eigenstrain on the vertex. Ru (1999) has proposed the celebrated works with conformal mapping with analytical continuation for arbitrarily shaped inhomogeneities for 2-D elastic problems in entire and semi-infinite space. Rather than using Eshelby's equivalent inclusion method, Ru focused on continuous equations on the boundary, but the solution is highly dependent on the auxiliary function. Subsequently, Ru (2000) has extended the solution scheme with conformal mapping for piezoelectric problems. Particularly, Wang and Schiavone (2021) have suggested the difficulty of determining exterior fields of inhomogeneity as it requires a completely determined auxiliary function involving the inverse mapping function. Zou et al. (2010) investigated non-elliptical inclusions for 2-D problems, including using the Laurent polynomials and polygons to characterize the arbitrarily shaped geometric shapes. The authors further calculated the spatially averaged Eshelby's tensor for micromechanical models, such as comparing ellipse-approximated particles. In addition, Zou et al. (2012) investigated the boundary effects of a finite domain with prescribed boundary conditions on an arbitrarily shaped inclusion. The authors adopted a popular method, the complex variable method, for 2-D analysis, and the problem was solved in a superposition scheme. Subsequently, Zou and He (2017) extended a similar superposition scheme for eccentric spherical inclusion embedded in a finite spherical body.

Although Eshelby's solution of ellipsoids with specific aspect ratios can be applied to investigate several interesting inhomogeneities or crack problems, such treatments are generally restricted by geometry shapes. They cannot be generalized to angular inhomogeneities such as triangular inhomogeneities. According to Rodin's work (Rodin, 1996) and our recent progress on polygonal inclusions (Wu and Yin, 2021), given a continuous and differentiable eigenstrain field, stress/strain fields around the vertex exhibit  $\ln r$  singularity. In such a case, if the classic slit-like crack is simulated by a triangular void with an adjusted aspect ratio, such as opening angle  $2\beta \to 0$  in Fig. 1, the previous conclusion of uniform eigenstrain by adjusted ellipsoidal does not hold for triangular inhomogeneities due to inconsistent singularity orders for interior and exterior observing points.

Such phenomenon can be interpreted as different geometric functions that ellipsoids are described with quadratic functions, while triangles exhibit sharp tips. Indeed, using a polynomial eigenstrain can rapidly estimate the solution. However, it may not approach the exact solution by simply increasing the order of polynomial eigenstrain due to the singularity of Eshelby's tensor at the vertices (Zou and Zheng, 2012). Because the variation of eigenstrain is localized in the neighborhood of the vertices, it is inefficient to represent the variation of eigenstrain through a single polynomial function. For example, the quarter-node elements have been extensively applied in the boundary element and finite element methods to simulate slit-like crack problems, as its shape function exhibits  $\sqrt{r}$  distribution (Portela et al., 1993). However, such numerical treatment requires a preliminary understanding of the singular behavior of elastic fields around the tip. Hence, it is critical to understand the eigenstrain distribution and interior/exterior elastic fields around the tip of the triangular inhomogeneity to integrate them into those numerical treatments (Aliabadi, 2002).

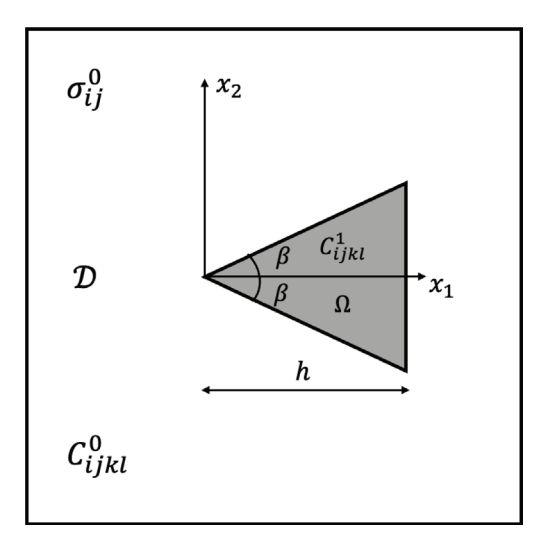


Fig. 1. Schematic illustration of a triangular inhomogeneity  $\Omega$  with angle  $2\beta$  and height h embedded in an unbounded matrix D subjected to far-field load  $\sigma_{ij}^0$ .

This paper focuses on the singularity on the top vertex of an isosceles triangle embedded in an unbounded matrix under uniform far-field load. Using Airy's stress function, the biharmonic potential functions can be expressed by separating variables. In such a case, the mechanical stress components within the inhomogeneity can be expressed by functions of distance and angle. Following Eshelby's equivalent inclusion method (EIM), the triangular inhomogeneity can be replaced by an inclusion with an eigenstrain field. Combining mechanical stress with Airy's stress function, one can derive the eigenstrain through the equivalent stress conditions in terms of stiffness tensors of the matrix and inhomogeneity. Through domain integrals of the eigenstrain with the modified Green's function, the disturbed strain and eigenstrain can be again associated through the equivalent stress condition, and the dominant terms are isolated through the series expansion. Through solving the eigenvalue problem, the singular eigenstrain and elastic distribution near the inhomogeneity tip can be obtained.

Note that this paper is fundamentally different from previous inclusion problems in the literature (Rodin, 1996; Gao and Liu, 2012; Wu and Yin, 2021; Wu et al., 2021), which investigated angular inclusion problems with a uniform or polynomial eigenstrain that cannot exactly satisfy the equivalent inclusion condition. This paper investigates an angular inclusion with a singular eigenstrain instead to meet the equivalent inclusion condition, and thus capture the singularity around the vertex.

In the following, Section 2 firstly introduces the boundary value problem (BVP) with the interface continuity. Subsequently, the EIM formulations and equivalent stress conditions are provided. Airy's stress functions are briefly reviewed, and the equivalent stress conditions are converted into integral equations. The domain integrals of Green's function with a singular source or eigenstrain field are derived from the dominant term. Section 3 verifies the method through comparison with the classic slit-like problem and explains the consistency of singularity order. Then, the method is applied to a general triangular void with different opening angles. Section 4 discusses the stress singularity for the general triangular inhomogeneity with different stiffness and angles under different loading conditions. Particularly, when the opening angle is zero, the triangular inhomogeneity becomes an interface glued by an adhesive. The stress singularity is studied. Section 5 provides some remarks of the significant results of this work and future extensions.

# 2. Formulation

## 2.1. Problem statement

Consider an inhomogeneity  $\Omega$  in the shape of an isosceles triangle with the opening angle  $2\beta$  and height h embedded in an infinite domain D subjected to a far-field load  $\sigma_{ij}^0$  shown as Fig. 1 in the Cartesian coordinate of the  $x_1-x_2$  plane with the origin at the top vertex. The matrix domain is denoted by  $D-\Omega$ . It can be either plane stress or plane strain problem. This paper uses plane strain for the formulation, in which the triangular inhomogeneities can be considered as a long prism with a triangular cross-section. For the isotropic elastic medium, let  $C_{ijkl}^I = \lambda^I \delta_{ij} \delta_{kl} + \mu^I (\delta_{ik} \delta_{jl} + \delta_{il} \delta_{jk})$ , where  $\lambda^I$  and  $\mu^I$  denote the Lame constants of the Ith phase of the composite, where I=0 or 1 representing the matrix and the inhomogeneity, respectively. The governing equations can be written as

$$C_{ijkl}^{I}(u_{k,li} - \varepsilon_{kl,i}^{*}) = 0 \quad \text{for } \mathbf{x} \in \mathcal{D}$$

Assume the interfaces are fully bonded. The boundary value problem of inhomogeneities could be enacted with the continuity equations of displacements and tractions as follows.

$$\sigma_{ij}^{+}(\mathbf{x})n_{i}^{+} = \sigma_{ij}^{-}(\mathbf{x})n_{i}^{-}, \quad u_{i}^{+}(\mathbf{x}) = u_{i}^{-}(\mathbf{x}) \quad \text{on} \quad \partial\Omega$$
 (2)

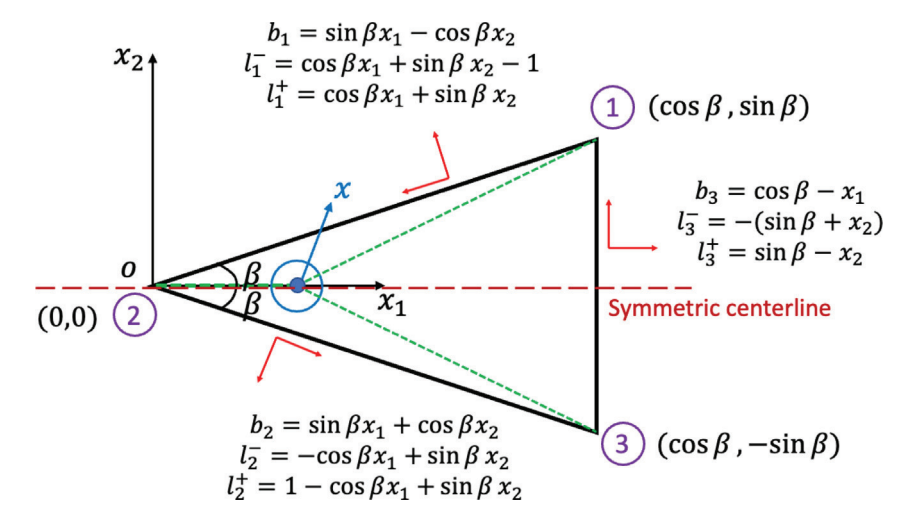


Fig. 2. Domain integral of potential functions over a triangle by three sub-triangles with the transformed coordinate, including edge-based directional and normal vector,  $b_f$  and  $l_{\pm}^{\pm}$ .

where  $\partial\Omega$  represents the interface between the inhomogeneity and the matrix; superscript + and – denote the outer and inner surface of the interface, respectively;  $n_j$  is the unit normal vector of the surface. Note that Dempsey and Sinclair (1979) considered other interfacial discontinuities for wedge problems as well, including smooth or rigid surfaces, which lead to 10 combinations by 4 types of interface conditions. Although the inhomogeneity problem shares some similarity with the wedge problem (Mura, 1987; Dempsey and Sinclair, 1979), the logarithmic singularity in the wedge problem is not commonly observed in the inhomogeneity problem with fully bonded interface, which will be revisited subsequently.

#### 2.2. Elastic fields caused by uniformly distributed eigenstrain

The isotropic elastic Green's function  $G_{ij}(\mathbf{x}, \mathbf{x}')$  can be expressed through combination of harmonic  $\phi$  and biharmonic  $\psi$  potentials as Eq. (3),

$$G_{ij}(\mathbf{x}, \mathbf{x}') = \frac{1}{4\pi\mu} \left[ \delta_{ij}\phi - \frac{1}{4(1-\nu)}\psi_{,ij} \right]$$
(3)

where  $\phi = -2 \ln |\mathbf{x} - \mathbf{x}'|$  and  $\psi = \frac{\phi - 1}{2} |\mathbf{x} - \mathbf{x}'|^2$ . Since this paper focuses on the plane strain problem, readers can switch conclusions for the plane stress problem by adjusting material properties. Following the definition of Green's function and source fields, disturbed elastic fields by uniformly distributed eigenstrain  $\varepsilon_{ii}^*$  can be derived through domain integrals as Eq. (4),

$$u_i(\mathbf{x}) = \int_{\Omega} g_{ikl}(\mathbf{x}, \mathbf{x}') \varepsilon_{kl}^*(\mathbf{x}') d\mathbf{x}' \quad \text{and} \quad \varepsilon_{ij}(\mathbf{x}) = \int_{\Omega} s_{ijkl}(\mathbf{x}, \mathbf{x}') \varepsilon_{kl}^*(\mathbf{x}') d\mathbf{x}'$$
(4)

where the modified Green's functions  $g_{ikl}$  and  $s_{ijkl}$  are shown as follows (Kröner, 1990),

$$g_{ikl} = \frac{1}{8\pi(1-v)} \left\{ \psi_{,ikl} - 2v\phi_{,i}\delta_{kl} - 2(1-v)(\phi_{,k}\delta_{il} + \phi_{,}\delta_{ik}) \right\}$$

$$s_{ijkl} = \frac{1}{8\pi(1-v)} \left\{ \psi_{,klij} - 2v\phi_{,ij}\delta_{kl} - (1-v)(\phi_{,kj}\delta_{il} + \phi_{,ki}\delta_{jl} + \phi_{,lj}\delta_{ik} + \phi_{,li}\delta_{jk}) \right\}$$
(5)

in which  $g_{ikl} = -G_{im,n}C_{mnkl}$  and  $s_{ijkl} = \frac{g_{ikl,j} + g_{jkl,i}}{2} = -\frac{(G_{im,nj} + G_{jm,ni})C_{mnkl}}{2}$  (Yin et al., 2022). Based on the identity of the elastic Green's function (Yin and Zhao, 2016),

$$C_{ijkl}\frac{G_{km,li} + G_{lm,ki}}{2} = C_{ijkl}G_{km,li} = -\delta_{jm}\delta(\mathbf{x} - \mathbf{x'})$$
(6)

where  $\delta(\mathbf{x}-\mathbf{x}')$  is the Dirac Delta function. Comparing Eq. (6) with the modified Green's function  $s_{ijkl}$  (Kröner, 1990), the following equations can be obtained as  $s_{ijml} = \delta_{jm}\delta(\mathbf{x}-\mathbf{x}')$  and  $s_{ijjl} = N\delta(\mathbf{x}-\mathbf{x}')$  with N=2 or 3 for 2D or 3D problem, respectively. The integral of  $s_{ijkl}$  is called the Eshelby's tensor  $S_{ijkl}$  to show the disturbed elastic field caused by a uniformly distributed eigenstrain, which exhibits a discontinuity across a smooth boundary with the norm vector  $\mathbf{n}$  as (Yin et al., 2022; Ju and Sun, 1999):

$$S_{ijkl}^{D}(\mathbf{n}) = S_{ijkl}^{+} - S_{ijkl}^{-} = \frac{1}{1 - v} n_i n_j n_k n_l - \frac{v}{1 - v} \delta_{kl} n_i n_j - \frac{1}{2} (\delta_{ik} n_j n_l + \delta_{il} n_j n_k + \delta_{jk} n_i n_l + \delta_{jl} n_i n_k)$$
(7)

Eq. (7) is applicable to both 2D and 3D cases, and tensor  $S^D$  is generated by the singular part of the Dirac Delta function of  $s_{ijkl}$  as discussed above. Using the Dirac measure property (Yin et al., 2022) in Eq. (4), one can write the strain discontinuity on the

boundary point x of the inclusion as:

$$\varepsilon_{ii}^{D}(\mathbf{x}) = S_{iikl}^{D}(\mathbf{n})\varepsilon_{kl}^{*}(\mathbf{x}) \tag{8}$$

which can be transferred to the stress discontinuity with the constitutive law (Mura, 1987; Yin et al., 2022) although the traction continuity in Eq. (2) shall be satisfied. The strain discontinuity over the boundary point is proportional to the eigenstrain on the point itself, as the eigenstrain source on other points always produces a continuous strain on x without any discontinuity.

Note that when the eigenstrain in an inclusion is not uniformly but continuously distributed, Eq. (8) is still applicable. This property creates an approach to solve the stress or strain on the inner boundary points while avoiding the singularity integral of the source on the point.

For a triangular inclusion  $\Omega$  shown in Fig. 1, Eshelby's tensor can be evaluated analytically as follows (Rodin, 1996; Wu and Yin, 2021): in Fig. 2, the triangle is divided into three elementary triangles by each edge. Using the transformed coordinate system for the integral over each triangle, the Eshelby's tensor can be analytically derived. Since this paper mainly focuses on the singular behaviors of the triangular tip,  $h = \cos \beta$  is selected for compact expressions of equations assuming the side edge length at 1.

Following the recent work (Wu and Yin, 2021), Eshelby's tensors along the symmetric line can be derived explicitly. Since the singular behavior of the triangular tip is of our interest, observing points are set along the symmetric centerline, i.e.,  $\mathbf{x} = (x_1, 0)$  and the tip behaviors can be acquired through limiting  $x_1 \to 0$ . With lengthy but straightforward derivation, Eshelby's tensor components  $S_{1111}, S_{1122}, S_{2211}, S_{2222}$  and  $S_{1212}$  can be written as follows:

$$\begin{split} S_{1111} &= -\frac{1}{4\pi(1-v)} \left\{ -(1-v) \left[ 4\beta + \sin 2\beta \ln(x_1^2) \right] - 2\sin^2\beta \left(\cos 2\beta - 2v + 3\right) \right. \\ &\left. \left[ \frac{\pi}{2} - \beta - \tan^{-1} \left( \cot\beta - \frac{\cos\beta}{x_1} \right) \right] - \frac{1}{4} \sin 4\beta \left[ \ln\left(x_1^2\right) + 2 \right] \right. \right\} \\ S_{1122} &= -\frac{1}{16\pi(1-v)} \left\{ -4v \left[ 4\beta + \sin 2\beta \ln(x_1^2) \right] + 8\sin^2\beta \left(\cos 2\beta - 2v + 1\right) \right. \\ &\left. \left[ \frac{\pi}{2} - \beta - \tan^{-1} \left( \cot\beta - \frac{\cos\beta}{x_1} \right) \right] + \sin 4\beta \left[ \ln\left(x_1^2\right) + 2 \right] \right. \right\} \\ S_{2211} &= -\frac{\cos\beta}{4\pi(1-v)} \left\{ \sin\beta \left[ 2\cos 2\beta + \ln\left(x_1^2\right) \left(\cos 2\beta + 2v\right) \right] - 2\cos\beta \left(\cos 2\beta + 2v - 1\right) \right. \\ &\left. \left[ \frac{\pi}{2} - \beta - \tan^{-1} \left( \cot\beta - \frac{\cos\beta}{x_1} \right) \right] \right. \right\} \\ S_{2222} &= -\frac{\cos\beta}{4\pi(1-v)} \left\{ 2\cos\beta \left( \cos 2\beta + 2v - 3 \right) \left[ \frac{\pi}{2} - \beta - \tan^{-1} \left( \cot\beta - \frac{\csc\beta}{x_1} \right) \right] \\ &- \sin\beta \left[ 2\cos 2\beta + \ln\left(x_1^2\right) \left( \cos 2\beta + 2v - 2 \right) \right] \right. \right\} \\ S_{1212} &= -\frac{1}{16\pi(1-v)} \left\{ -8(1-v)\cot^{-1} \left( \cot\beta - x_1\csc\beta \right) - 2(\cos 4\beta - 4v + 3) \right. \\ &\left. \left[ \frac{\pi}{2} - \beta - \tan^{-1} \left( \cot\beta - \frac{\csc\beta}{x_1} \right) \right] + \sin 4\beta \left[ \ln\left(x_1^2\right) + 2 \right] \right. \right\} \end{split}$$

As shown in Eq. (9), the singularity terms of at  $x_1 \to 0^+$  and  $x_1 \to 0^-$  shall be carefully addressed as they change signs for the integral in the transformed coordinate at the two sides of the origin.

(I) Interior Cases:  $x_1 \rightarrow 0^+$ 

Simplifying Eq. (9) by limiting  $x_1 \to 0^+$ , five Eshelby's tensors can be rewritten as,

$$S_{1111} = \frac{2(\pi - \beta)\sin^{2}\beta(\cos 2\beta - 2\nu + 3) + (1 - \nu)\left[4\beta + \sin 2\beta \ln\left(x_{1}^{2}\right)\right] + \frac{1}{4}\sin 4\beta\left[\ln\left(x_{1}^{2}\right) + 2\right]}{4\pi(1 - \nu)}$$

$$S_{1122} = \frac{-8(\pi - \beta)\sin^{2}\beta(\cos 2\beta - 2\nu + 1) + 4\nu\left[4\beta + \sin 2\beta \ln\left(x_{1}^{2}\right)\right] - \sin 4\beta\left[\ln\left(x_{1}^{2}\right) + 2\right]}{16\pi(1 - \nu)}$$

$$S_{2211} = \frac{-\cos\beta\left(\sin\beta\left[2\cos 2\beta + \ln\left(x_{1}^{2}\right)(\cos 2\beta + 2\nu)\right] + 2(\pi - \beta)\cos\beta(\cos 2\beta + 2\nu - 1)\right)}{4\pi(1 - \nu)}$$

$$S_{2222} = \frac{-\cos\beta\left(2(\pi - \beta)\cos\beta(\cos 2\beta + 2\nu - 3) - \sin\beta\left[2\cos 2\beta + \ln\left(x_{1}^{2}\right)(\cos 2\beta + 2\nu - 2)\right]\right)}{4\pi(1 - \nu)}$$

$$S_{1212} = \frac{2\beta - 2(\beta - \pi)\cos 4\beta - 2\pi(4\nu - 3) - \sin 4\beta\left[\ln\left(x_{1}^{2}\right) + 2\right]}{16\pi(1 - \nu)}$$

$$(10)$$

(II) Exterior Cases:  $x_1 \rightarrow 0^-$ 

$$\begin{split} S_{1111} &= \frac{-\cos\beta\left(-2\beta\cos\beta(\cos2\beta-2\upsilon+1)-\sin\beta\left[2\cos2\beta+\ln\left(x_1^2\right)(\cos2\beta-2\upsilon+2)\right]\right)}{4\pi(1-\upsilon)} \\ S_{1122} &= \frac{-\sin4\beta\left[\ln\left(x_1^2\right)+2\right]+4\cos\beta\left[-\beta\cos3\beta+\beta(4\upsilon+1)\cos\beta+2\upsilon\sin\beta\ln\left(x_1^2\right)\right]}{16\pi(1-\upsilon)} \end{split}$$

$$S_{2211} = \frac{-\cos\beta \left(2\beta\cos\beta(\cos2\beta + 2\nu - 1) + \sin\beta \left[2\cos2\beta + \ln\left(x_1^2\right)(\cos2\beta + 2\nu\right)\right]\right)}{4\pi(1 - \nu)}$$

$$S_{2222} = \frac{\cos\beta \left(2\beta\cos\beta(\cos2\beta + 2\nu - 3) + \sin\beta \left[2\cos2\beta + \ln\left(x_1^2\right)(\cos2\beta + 2\nu - 2)\right]\right)}{4\pi(1 - \nu)}$$

$$S_{1212} = \frac{-\sin4\beta \left[\ln\left(x_1^2\right) + 2\right] + 4\beta\sin^22\beta}{16\pi(1 - \nu)}$$
(11)

In Eqs. (10) and (11), both interior and exterior cases exhibit logarithmic singularities when  $x_1 \to 0$  with uniformly distributed eigenstrain in the triangular inclusion. Subtracting Eqs. (10) by (11), the difference of Eshelby's tensor  $S^D$  on the vertex point can be obtained.

$$S_{1111}^{D} = \frac{\sin^{2}\beta(\cos2\beta - 2\nu + 3)}{2(1 - \nu)}; \quad S_{1122}^{D} = -\frac{\sin^{2}\beta(\cos2\beta - 2\nu + 1)}{2(1 - \nu)}$$

$$S_{2211}^{D} = \frac{\cos^{2}\beta(\cos2\beta + 2\nu - 1)}{2(1 - \nu)}; \quad S_{2222}^{D} = -\frac{\cos^{2}\beta(\cos2\beta + 2\nu - 3)}{2(1 - \nu)}$$

$$S_{1212}^{D} = -\frac{\cos4\beta - 4\nu + 3}{8(1 - \nu)}$$

$$(12)$$

where all unlisted components are zero. Alternatively, Eq. (12) can be derived through Eq. (7) as follows: since the vertex involves two branches of discontinuity, the upper and lower edge, whose normal vectors are  $n^u = (-\sin\beta, \cos\beta)$  and  $n^l = -(\sin\beta, \cos\beta)$ , respectively. The difference of the Eshelby's tensor for the upper and lower edges are obtained from Eq. (7) as:

$$S_{1111}^{Du} = S_{1111}^{Dl} = \frac{\sin^2 \beta(\cos 2\beta - 2\nu + 3)}{2(1 - \nu)}; \quad S_{1122}^{Du} = S_{1122}^{Dl} = -\frac{\sin^2 \beta(\cos 2\beta - 2\nu + 1)}{2(1 - \nu)}$$

$$S_{2211}^{Du} = S_{2211}^{Dl} = \frac{\cos^2 \beta(\cos 2\beta + 2\nu - 1)}{2(1 - \nu)}; \quad S_{2222}^{Du} = S_{2222}^{Dl} = -\frac{\cos^2 \beta(\cos 2\beta + 2\nu - 3)}{2(1 - \nu)}$$

$$S_{1212}^{Du} = S_{1212}^{Dl} = -\frac{\cos 4\beta - 4\nu + 3}{8(1 - \nu)}; \quad S_{1211}^{Du} = -S_{1211}^{Dl} = \frac{\sin \beta \cos \beta \left(\sin^2 \beta + \nu - 1\right)}{1 - \nu}; \quad S_{1211}^{Du} = -S_{1211}^{Dl} = \frac{\sin \beta \cos^3 \beta}{1 - \nu}$$

$$S_{1222}^{Du} = -S_{1222}^{Dl} = \frac{\sin^3 \beta \cos \beta}{1 - \nu}; \quad S_{2212}^{Du} = -S_{2212}^{Dl} = -\frac{\sin \beta \cos \beta \left(\cos^2 \beta + \nu - 1\right)}{1 - \nu}$$

$$(13)$$

where superscripts "Du" and "Dl" denote the difference along the upper and lower edges, respectively. Because the surface norm at the vertex is not well defined yet, Eq. (7) cannot be directly used. However, as Eq. (13) exhibits the five components of  $S^D$  in Eq. (12) are the same for both calculation from the upper and lower edges, and the other components have the opposite signs, i.e.,  $S_{1112}^{Du} = -S_{1112}^{Dl}$ , one can conclude:

$$S_{ijkl}^{D} = \frac{S_{ijkl}^{Du} + S_{ijkl}^{Dl}}{2} \tag{14}$$

The derivation of all components are provided as script with the Supplemental Materials of "Discontinuity of Eshelby's tensor.nb". Although the Eshelby's tensor exhibits a logarithmic singularity at the vertex, all components of  $S^D$  are finite, because the integral of a Dirac Delta function leads to a Heaviside function (Yin et al., 2022). Therefore, if the strain at the outside boundary of the inclusion is obtained, the one at the inside boundary can also be obtained by the superposition of the strain at the outer boundary point and the discontinuity in Eq. (8).

When Eshelby's EIM is used, the eigenstrain shall be determined by the stress equivalent condition in the next subsection. For a particle with a uniform stiffness, the eigenstrain shall be continuous in the equivalent inclusion, but the eigenstrain on the boundary or vertex is still open to question. An asymptotic elastic analysis can be utilized to determine the eigenstrain and elastic field.

# 2.3. Equivalent stress conditions

When the inhomogeneity  $\Omega$  is replaced with the matrix and a continuously distributed eigenstrain, Eshelby's equivalent stress condition can be constructed as (Mura, 1987):

$$C_{ijkl}^{0}(\varepsilon_{kl}^{0} + \varepsilon_{kl}' - \varepsilon_{kl}^{*}) = C_{ijkl}^{1}(\varepsilon_{kl}^{0} + \varepsilon_{kl}')$$

$$\tag{15}$$

where  $\epsilon_{kl}^0$  and  $\epsilon_{kl}'$  are uniform far-field load and disturbed strain caused by eigenstrain in Eq. (4), respectively. Notice that eigenstrain is a function of source point  $\mathbf{x}'$ . For an ellipsoidal inhomogeneity in the infinite domain, the Eshelby's tensor in the interior domain is constant, and thus the eigenstrain will be uniform in the inhomogeneity domain. However, a uniform eigenstrain may never satisfy the equivalent stress condition of Eq. (15) at the neighborhood of the vertex for a triangular inhomogeneity because the Eshelby tensor becomes singular. Hence, for general cases, directly using uniform or polynomial eigenstrain usually results in inaccurate predictions for polygonal inhomogeneities (Wu and Yin, 2021), particularly in the neighborhood of the vertices. Discretization of

particles may provide tailorable accuracy (Wu et al., 2021), but it comes with a high computational cost and an unknown convergent rate. Therefore, it is critical to investigate and understand the distributions of eigenstrain in the neighborhood of the vertex.

The eigenstrain in the exact solution of this inhomogeneity problem shall satisfy the equivalent stress condition of Eq. (15) at every point in the triangular inhomogeneity. A polynomial or piecewise continuous eigenstrain function can provide satisfactory results for the interior points, but can never exactly satisfy the stress equivalence at the vertex. An asymptotic elastic analysis shall be used to address the singularity of the stress components, which may achieve the stress equivalence at the vertex in an analytical fashion.

Williams (1952) and Dempsey and Sinclair (1979) proposed to use the separation of variables to express the biharmonic potentials of Airy's stress function, which is briefly reviewed as below. Consider a biharmonic potential V governed by the strain compatibility law that  $\nabla^4 V = 0$ . The displacement and stress components in the polar coordinate can be expressed as,

$$2\mu u_{r} = -V_{,r} + (1 - v)rV_{,\theta}; \quad 2\mu u_{\theta} = -\frac{1}{r}V_{,\theta} + (1 - v)r^{2}V_{,r}$$

$$\sigma_{rr} = \frac{1}{r}V_{,r} + \frac{1}{r^{2}}V_{,\theta\theta}; \quad \sigma_{\theta\theta} = V_{,rr}; \quad \sigma_{r\theta} = \frac{1}{r^{2}}V_{,\theta} - \frac{1}{r}V_{,r\theta}$$
(16)

In general, Airy's stress function is constructed with the boundary conditions. Following Dempsey and Sinclair's notation, one can write the displacements and stresses in the following form:

$$\mathbf{u} = \begin{bmatrix} u_r \\ u_\theta \end{bmatrix} = \frac{\partial}{\partial \lambda} \left\{ r^{1-\lambda} \left[ U(\theta, \lambda) c(\lambda) \right] \right\}; \quad \mathbf{\sigma} = \begin{bmatrix} \sigma_{rr} \\ \sigma_{r\theta} \\ \sigma_{\theta\theta} \end{bmatrix} = \frac{\partial}{\partial \lambda} \left\{ r^{-\lambda} \left[ S(\theta, \lambda) c(\lambda) \right] \right\}$$
(17)

where  $c(\lambda)$  is a coefficient list of 4 components to be determined by the boundary conditions. Notice that Dempsey and Sinclair introduce  $\partial/\partial\lambda$  to consider the logarithmic singularities for composite wedge, and the logarithmic singularity may not exist for all cases. Based on the bounded energy criteria (Barber, 1992), the singularity parameter  $\lambda < 1$ .

$$U = \begin{bmatrix} (\lambda - 2)p + (1 - v)q_{,\theta\theta} \\ -p_{,\theta} - (1 - v)\lambda q \end{bmatrix}; \quad S = \begin{bmatrix} (2 - \lambda)p + p_{,\theta\theta} \\ -(1 - \lambda)p_{,\theta} \\ (2 - \lambda)(1 - \lambda)p \end{bmatrix}$$

$$p = \left[\sin(2 - \lambda)\theta, \cos(2 - \lambda)\theta, \sin\lambda\theta, \cos\lambda\theta\right]; \quad q = \begin{bmatrix} 0, & 0, & \frac{-4}{\lambda}\cos\lambda\theta, & \frac{4}{\lambda}\sin\lambda\theta \end{bmatrix}$$

$$(18)$$

In an explicit form, the stress components in the polar coordinate can be written as,

$$\sigma_{rr} = \frac{\partial}{\partial \lambda} \left\{ r^{-\lambda} (-1 + \lambda) \left[ c_1(\lambda)(2 - \lambda) \sin(2 - \lambda)\theta + c_2(\lambda)(2 - \lambda) \cos(2 - \lambda)\theta \right. \right.$$

$$\left. - c_3(\lambda)(\lambda + 2) \sin \lambda \theta - c_4(\lambda)(\lambda + 2) \cos \lambda \theta \left. \right] \right\}$$

$$\sigma_{\theta\theta} = \frac{\partial}{\partial \lambda} \left\{ r^{-\lambda} (1 - \lambda)(2 - \lambda) \left[ c_1(\lambda) \sin(2 - \lambda)\theta + c_2(\lambda) \cos(2 - \lambda)\theta + c_3(\lambda) \sin \lambda \theta + c_4(\lambda) \cos \lambda \theta \right. \right] \right\}$$

$$\sigma_{r\theta} = \frac{\partial}{\partial \lambda} \left\{ r^{-\lambda} (-1 + \lambda) \left[ c_1(\lambda)(2 - \lambda) \cos(2 - \lambda)\theta - (2 - \lambda)c_2(\lambda) \sin(2 - \lambda)\theta + c_3(\lambda)\lambda \cos \lambda \theta - c_4(\lambda)\lambda \sin \lambda \theta \right. \right] \right\}$$

$$(19)$$

The constitutive law is written in terms of either the actual material or the equivalent inclusion as:

$$\varepsilon_{ij}^{0} + \varepsilon_{ij}' = (C_{ijkl}^{1})^{-1} \sigma_{kl}; \quad \varepsilon_{ij}^{0} + \varepsilon_{ij}' - \varepsilon_{ij}^{*} = (C_{ijkl}^{0})^{-1} \sigma_{kl}$$
(20)

For a 2D problem, the stiffness tensor  $C_{ijkl} = 2KI^d_{ijkl} + 2\mu I^h_{ijkl}$ , where  $I^d_{ijkl} \equiv \frac{\delta_{ij}\delta_{kl}}{2}$ ;  $I^h_{ijkl} \equiv \frac{\delta_{ik}\delta_{jl} + \delta_{il}\delta_{jk}}{2} - I^d_{ijkl}$ ; and K is the bulk modulus (Yin and Zhao, 2016). Hence, the relation between the eigenstrain and stress on the inhomogeneity domain can be formulated as:

$$\varepsilon_{ij}^* = (C_{ijkl}^0)^{-1} (C_{klmn}^0 - C_{klmn}^1) (C_{mnsi}^1)^{-1} \sigma_{st} = \left(\frac{K^0 - K^1}{2K^0 K^1} I_{ijkl}^d + \frac{\mu^0 - \mu^1}{2\mu^0 \mu^1} I_{ijkl}^h\right) \sigma_{kl}$$
(21)

In general, the eigenstrain due to the material mismatch shares the same order of the singularity as the stress in the inhomogeneity around the vertex when the stiffness of the inhomogeneity is not zero. Mathematically, the problem is reduced to search the eigenstrain at the appropriate singularity parameter  $\lambda$  that lead to the stress sharing the same singularity parameter around the vertex to meet the stress equivalent condition in Eq. (15). For different shape, stiffness ratio, and loading conditions,  $\lambda$  can be different. For example, for an ellipsoidal inhomogeneity,  $\lambda$  becomes zero as a uniform eigenstrain can produce a uniform stress field in the inhomogeneity (Mura, 1987; Yuan and Liu, 2023). However, for a polygonal inhomogeneity, a uniform eigenstrain produces a stress field with a  $\ln(r)$  singularity (Rodin, 1996; Yin et al., 2022). Therefore, the singularity parameter of a triangular inhomogeneity is surely not zero, but needs to be determined by the stress equivalent conditions and loading conditions.

By writing bulk modulus K in terms of shear modulus  $\mu$  and Poisson's ratio  $\nu$ , the eigenstrain components in the polar coordinate can be written as,

$$\begin{split} \varepsilon_{rr}^* &= -\frac{\partial}{\partial \lambda} \left\{ \ \frac{\lambda-1}{2\mu^0\mu^1} r^{-\lambda} \left[ \ c_1(\lambda-2)(\mu^0-\mu^1) \sin(2-\lambda)\theta + c_2(\lambda-2)(\mu^0-\mu^1) \cos(\lambda-2)\theta \right. \right. \\ & \left. - \left. \left( c_3 \sin \lambda \theta + c_4 \cos \lambda \theta \right) (\mu^1(\lambda-4v^0+2) + \mu^0(-\lambda+4v^1-2)) \ \right] \right\} \end{split}$$

$$\begin{split} & \varepsilon_{r\theta}^* = \frac{\partial}{\partial \lambda} \left\{ \frac{(\lambda - 1)(\mu^0 - \mu^1)}{2\mu^0 \mu^1} r^{-\lambda} \left[ -c_4 \lambda \sin \lambda \theta + c_3 \lambda \cos \lambda \theta - \left( (\lambda - 2) \left( c_2 \sin(\lambda - 2) \theta + c_1 \cos(\lambda - 2) \theta \right) \right) \right] \right\} \\ & \varepsilon_{\theta\theta}^* = \frac{\partial}{\partial \lambda} \left\{ \frac{\lambda - 1}{2\mu^0 \mu^1} r^{-\lambda} \left[ c_1 (\lambda - 2)(\mu^0 - \mu^1) \sin(2 - \lambda) \theta + c_2 (\lambda - 2)(\mu^0 - \mu^1) \cos(\lambda - 2) \theta \right. \right. \\ & \left. + \left( c_3 \sin \lambda \theta + c_4 \cos \lambda \theta \right) (\mu^0 (\lambda + 4v^1 - 2) - \mu^1 (\lambda + 4v^0 - 2)) \right] \right\} \end{split}$$

Based on Eq. (15), the integral equation between disturbed strain and eigenstrain can be used to derive the stress as

$$\sigma_{ij} = C_{ijkl}^0 \left( \varepsilon_{kl}^0 + \int_O s_{klmn}(\mathbf{x}, \mathbf{x}') \varepsilon_{mn}^*(\mathbf{x}') \, d\mathbf{x}' - \varepsilon_{kl}^* \right) \tag{23}$$

As the form of stress  $\sigma$  and eigenstrain  $\varepsilon^*$  are given in terms of  $\lambda$  and coefficients  $c_i$  (i = 1, 2, 3, 4), they can be determined from the above equation given the loading condition.

Although the stress and eigenstrain in the neighborhood of the vertex are given in the form of the Airy's stress function in Eqs. (19) and (22), respectively, the solution of this boundary value problem relies on the integral of the second term,  $s_{klmn}\epsilon_{mn}^*$ , in Eq. (23). Here  $\epsilon_{mn}^*$  is discontinuous along the boundary of the triangular domain and singular on the vertex, while the Eshelby's tensor  $S_{klmn}$  for the uniform eigenstrain also exhibits discontinuity along the boundary of the triangular domain and singularity on the vertex. The integral of  $s_{klmn}\epsilon_{mn}^*$  shall follow the same phenomenon and the discontinuity across the boundary can be described by Eq. (8), while Eshelby's tensor  $S_{klmn}$  and eigenstrain  $\epsilon_{mn}^*$  are continuous within the triangular domain.

#### 2.4. Stress discontinuity and singularity at the vertex

The integral equation of disturbed strain and eigenstrain, known as Fredholm's integral equation (Martin, 1991, 1992), has been well studied in the literature. Many efforts have been devoted to solving such equations in the one-dimensional domain, and numerical schemes are the popular choice for multi-dimensional problems. Since this paper focuses on the singular behavior of elastic fields around the tip, asymptotic analysis will be applied. To analyze the singular behavior of elastic fields in Eq. (23), it is necessary first to evaluate the domain integral of Green's function and with the varying eigenstrain. Although the authors (Wu and Yin, 2021) have applied the transform coordinates (TC) to simplify the domain integrals of polynomial eigenstrains, the integral scheme may not be efficient for source fields with power function distributions, because the form of the distance vector in the TC changes as the origin of the TC moves, which is different from the polynomial form of eigenstrain.

To appropriately evaluate the stress discontinuity and singularity at the vertex, in Fig. 2, one can calculate the strain at  $(0^-,0)$  or the left side of the origin. Because it is outside of the inhomogeneity, the Dirac Delta function in the Eshelby's tensor does not play any role, and the integral of  $s_{klmn}\epsilon_{mn}^*$  in Eq. (23) can be derived directly. As the stress equivalence condition is set up at the inside of the inhomogeneity or  $(0^+,0)$ , the discontinuity of the strain at the vertex will be used in terms of Eq. (12).

In the following, the strain at  $(0^-,0)$  will be firstly derived in terms of each component. Considering the global coordinate for the far field load, this section aims to conduct domain integral of Green's function and dominant terms of eigenstrain in the Cartesian coordinate. Without the loss of any generality, consider disturbed strain  $\varepsilon'_{11}$ , which contains domain integrals of  $\phi_{.11}\varepsilon^*_{.11}$ ,  $\phi_{.22}\varepsilon^*_{.22}$ ,  $\psi_{.1111}\varepsilon^*_{.11}$ ,  $\psi_{.1112}\varepsilon^*_{12}$  and so on. After a lengthy but straightforward derivation, these integrals can be explicitly obtained. For example,  $\phi_{.11}\varepsilon^*_{11}$  and  $\phi_{.22}\varepsilon^*_{22}$  are provided in this section, and other components are elaborated in Appendix B. For the simplicity of illustration, only normal stress coefficients are considered with  $c_1=c_3=0$ . Notice that the following integral does not contain contributions from the Dirac delta function, which has been handled with Eq. (8). Let  $\Omega^p$  represents the polar coordinate integral domain of the triangle with the observing point at the exterior of the vertex.

Integral of  $\phi_{,11} \varepsilon_{11}^*$ 

Based on Eq. (A.1) and Eq. (A.3),

$$\int_{\Omega^{p}} \phi_{,11} \varepsilon_{11}^{*} d\mathbf{x}' = \int_{-\beta}^{\beta} \int_{0}^{1} \frac{2 \left( r^{2} \cos 2\theta - 2rx_{1} \cos \theta + x_{1}^{2} \right)}{\left( r^{2} - 2rx_{1} \cos \theta + x_{1}^{2} \right)^{2}} \varepsilon_{11}^{*} r dr d\theta$$
(24)

where eigenstrain can be described as  $\varepsilon_{ij}^* = \frac{\partial [r^{-\lambda} H_{ij}(\lambda,\theta)]}{\partial \lambda}$ . The following three steps can be conducted to reach the explicit form of the integral: (i) integrate  $r^{-\lambda}$ ; (ii) conduct series expansion around the vertex and combine it with eigenstrain; and (iii) integrate the variable  $\theta$ .

Hence, step (i) of Eq. (24) yields as,

$$\int_{0}^{1} \phi_{,11} r^{1-\lambda} dr = \frac{2r^{2-\lambda}}{\lambda} \left( -\frac{(\lambda - 1)\lambda}{2(\lambda - 2)x_{1}^{2}} \left( {}_{2}F_{1} \left( 1, 2 - \lambda; 3 - \lambda; r \left[ \left( \cos \theta - \sqrt{-\sin^{2} \theta} \right) x_{1} \right]^{-1} \right) \right) + \frac{\lambda}{2} F_{1} \left( 1, 2 - \lambda; 3 - \lambda; r \left[ \left( \cos \theta + \sqrt{-\sin^{2} \theta} \right) x_{1} \right]^{-1} \right) \right) + \frac{\lambda}{r^{2} - 2rx_{1} \cos \theta + x_{1}^{2}} - \frac{\lambda r \cos \theta}{x_{1} \left( r^{2} - 2rx_{1} \cos \theta + x_{1}^{2} \right)} \right)$$

$$(25)$$

where  ${}_2F_1$  is the hypergeometric function. Based on the strain energy criteria ( $\lambda < 1$ ), when  $r \to 0$ , Eq. (25) yields as zero and thus the definite integral is only related to its upper limit  $r \to 1$ . To obtain elastic behaviors around the inhomogeneity tip, series

expansion with respect to  $x_1$  at 0 is conducted. Similar to Eshelby's tensor in Eq. (9), it is necessary to discuss two cases of  $x_1 \to 0^+$  and  $x_1 \to 0^-$  for interior and exterior observing points, respectively.

$$\int_{0}^{1} \phi_{,11} r^{1-\lambda} dr = \begin{cases} -\frac{2\cos 2\theta}{\lambda} - 2x_{1}^{-\lambda} \pi(\lambda - 1) \csc \lambda \pi \cos[\lambda \pi + \theta(2 - \lambda)] + \mathcal{O}(x_{1}^{3}) & x_{1} \to 0^{+} \\ -\frac{2\cos 2\theta}{\lambda} - 2|x_{1}|^{-\lambda} \pi(\lambda - 1) \csc \lambda \pi \cos[\theta(2 - \lambda)] + \mathcal{O}(|x_{1}|^{3}) & x_{1} \to 0^{-} \end{cases}$$
(26)

where  $-\frac{2\cos 2\theta}{\lambda}$  is from the far-end contribution, and the rest of terms with  $x_1^{-\lambda}$  is from the close-end contribution, which is closely related to singular behaviors around the tip. While the second branch determines exterior elastic behaviors, the interior ones can be obtained by the superposition with the difference tensor  $S^D$ , which is later applied to the equivalent stress conditions.

For illustration purposes, considering  $c_1 = c_3 = 0$  for symmetric loading cases, one can obtain the close-end contribution from the second branch with eigenstrain  $\varepsilon_{11}^*$  for step (ii) as follows:

$$-2|x_{1}|^{-\lambda}\pi(\lambda-1)\csc\lambda\pi\cos[\theta(2-\lambda)]H_{11}(\lambda,\theta) = |x_{1}|^{-\lambda}\frac{\pi(\lambda-1)^{2}\csc\lambda\pi}{\mu^{0}\mu^{1}}\cos[(2-\lambda)\theta] \left\{ c_{2}(\lambda-2)(\mu^{0}-\mu^{1})\cos\lambda\theta + c_{4}\left[\lambda(\mu^{0}-\mu^{1})\cos[(2+\lambda)\theta] + 2\cos\lambda\theta[\mu^{0}(1-2v^{1})-\mu^{1}(1-2v^{0})]\right] \right\}$$
(27)

Then the integral of Eq. (27) with respect to angle  $\theta \in [-\beta, \beta]$ , when  $x_1 \to 0^-$ , can be obtained as:

$$\begin{split} &\int_{\varOmega^{p}} \phi_{,11} r^{-\lambda} H_{11}(\lambda,\beta) d\mathbf{x}' = |x_{1}|^{-\lambda} \frac{\pi(\lambda-1) \csc(\pi\lambda)}{8\mu^{0}\mu^{1}} \left\{ 2c_{4}(\lambda-1)(\mu^{0}-v^{1}) \left[ \lambda \sin(\lambda\pi+4\beta) - 2\sin\lambda(\pi-2\beta) \right] \right. \\ & + \left[ 4(\lambda-1) \sin(\lambda\pi+2\beta) - 4\sin\left[ \lambda\pi+2\beta(1-\lambda) \right] \right] \left[ c_{2}(\lambda-2)(\mu^{0}-\mu^{1}) + 2c_{4} \left[ \mu^{0}(1-2v^{0}) - \mu^{1}(1-2v^{0}) \right] \right] \\ & + 2(2-\lambda) \sin\lambda\pi \left[ 2c_{2}(\lambda-2)(\mu^{0}-\mu^{1}) + c_{4} \left[ \mu^{1}(-\lambda+8v^{0}-3) + \mu^{0}(\lambda-8v^{1}+3) \right] \right] \right\} \end{split} \tag{28}$$

For cases with the logarithmic singularity, one can take the partial derivative of Eq. (28) with respect to  $\lambda$ . More discussion on the existence of logarithmic singularities is provided in Section 4.

Integral of  $\phi_{,22}\varepsilon_{,2}^*$ 

Based on Eqs. (A.1) and (A.3),

$$\int_{\Omega^{p}} \phi_{,22} \varepsilon_{22}^{*} d\mathbf{x}' = \int_{-\beta}^{\beta} \int_{0}^{1} -\frac{2 \left(r^{2} \cos 2\theta - 2rx_{1} \cos \theta + x_{1}^{2}\right)}{\left(r^{2} - 2rx_{1} \cos \theta + x_{1}^{2}\right)^{2}} \varepsilon_{22}^{*} r dr d\theta$$
(29)

Following the same fashion of the previous subsection, the integral of Eq. (29) in r can be obtained:

$$\int_{0}^{1} \phi_{,22} r^{1-\lambda} dr = \frac{2r^{2-\lambda}}{\lambda} \left( -\frac{(\lambda - 1)\lambda}{2(\lambda - 2)x_{1}^{2}} \left( {}_{2}F_{1} \left( 1, 2 - \lambda; 3 - \lambda; r \left[ \left( \cos \theta - \sqrt{-\sin^{2} \theta} \right) x_{1} \right]^{-1} \right) \right) + \frac{\lambda}{2} F_{1} \left( 1, 2 - \lambda; 3 - \lambda; r \left[ \left( \cos \theta + \sqrt{-\sin^{2} \theta} \right) x_{1} \right]^{-1} \right) \right) + \frac{\lambda}{r^{2} - 2rx_{1} \cos \theta + x_{1}^{2}} - \frac{\lambda r \cos \theta}{x_{1} \left( r^{2} - 2rx_{1} \cos \theta + x_{1}^{2} \right)} \right)$$
(30)

Similarly, expanding Eq. (30) with  $x_1$  for both interior and exterior points,

$$\int_{0}^{1} \phi_{,22} r^{1-\lambda} dr = \begin{cases} \frac{2\cos 2\theta}{\lambda} + 2x_{1}^{-\lambda} \pi(\lambda - 1)\csc \lambda \pi \cos[\lambda \pi + (2 - \lambda)\theta] + \mathcal{O}(x_{1}^{3}) & x_{1} \to 0^{+} \\ \frac{2\cos 2\theta}{\lambda} + 2|x_{1}|^{-\lambda} \pi(\lambda - 1)\csc \lambda \pi \cos[(2 - \lambda)\theta] + \mathcal{O}(|x_{1}|^{3}) & x_{1} \to 0^{-} \end{cases}$$
(31)

Multiplying the close-end contribution from first branch with eigenstrain  $H_{22}(\lambda,\theta)$ , the equation of step (ii) can be obtained,

$$2|x_{1}|^{-\lambda}\pi(\lambda-1)\csc\lambda\pi\cos[(2-\lambda)\theta]H_{22}(\lambda,\theta) = \frac{\pi(\lambda-1)^{2}\csc\lambda\pi\cos[(2-\lambda)\theta]}{\mu^{0}\mu^{1}} \left\{ c_{2}(\lambda-2)(\mu^{0}-\mu^{1})\cos\lambda\theta + c_{4}\left[\lambda(\mu^{0}-\mu^{1})\cos[(2+\lambda)\theta] - 2\cos\lambda\theta[\mu^{0}(1-2v^{1}) - \mu^{1}(1-2v^{0})]\right] \right\}$$
(32)

Therefore, one can obtain:

$$\int_{\Omega^{p}} \phi_{,22} H_{22}(\lambda,\beta) r^{-\lambda} d\mathbf{x}' = |x_{1}|^{-\lambda} \frac{\pi(\lambda - 1) \csc \lambda \pi}{4\mu^{0} \mu^{1}} \left\{ c_{4}(\lambda - 1)(\mu^{0} - \mu^{1}) \left[ \lambda \sin[\lambda \pi + 4\beta] - 2 \sin \lambda(\pi - 2\beta) \right] - 2 \left[ \sin[\lambda \pi + 2\beta(1 - \lambda)] - (\lambda - 1) \sin(\lambda \pi + 2\beta) \right] \left[ c_{2}(\lambda - 2)(\mu^{0} - \mu^{1}) - 2c_{4} \left[ \mu^{0}(1 - 2v^{1}) - \mu^{1}(1 - 2v^{0}) \right] \right] + (2 - \lambda) \sin \lambda \pi \left[ 2c_{2}(\lambda - 2)(\mu^{0} - \mu^{1}) + c_{4} \left[ \mu^{0}(\lambda + 8v^{1} - 5) - \mu^{1}(\lambda + 8v^{0} - 5) \right] \right] \right\}$$
(33)

After obtaining the integral from the polar coordinate of Green's function and dominant terms from eigenstrain, the next step is to consider the influence of eigenstrain at the interior vertex as the observing point. The contribution of Dirac delta function have been considered as Eq. (8). Hence, equivalent stress conditions of Eq. (23) can be rewritten as,

$$\sigma_{ij} = C_{ijkl}^0 \left[ \varepsilon_{kl}^0 + S_{klmn}^D \varepsilon_{mn}^*(\mathbf{x}) + \int_{\Omega^P} s_{klmn}(\mathbf{x}, \mathbf{x}') \varepsilon_{mn}^*(\mathbf{x}') d\mathbf{x}' - \varepsilon_{kl}^*(\mathbf{x}) \right]$$
(34)

where  $\int_{\Omega^P} s_{klmn}(\mathbf{x}, \mathbf{x}') \epsilon_{mn}^*(\mathbf{x}') d\mathbf{x}'$  can be obtained through the combination of the above polar coordinate integrals among other terms, which are elaborated in Appendix B. The similar procedure can be conducted for the shearing case of the antisymmetric problem with  $c_2 = c_4 = 0$ , and the integrals are provided in Appendix C. Therefore, the stress and eigenstrain can be determined by Eq. (34).

#### 3. Triangular void problems

Section 2 presents the boundary value problem of inhomogeneities and constructs integral equations among disturbed strain, eigenstrain, and stress components. The domain integral of Green's function and dominant terms of eigenstrain are calculated through the combination of uniform Eshelby's tensor and polar coordinate. In the following, the domain integrals are further applied to solve equivalent stress conditions for triangular voids.

# 3.1. Simplification of eigenstrain and domain integrals

The material properties of voids are  $\mu^1 = K^1 \to 0$ . The expression for eigenstrain and domain integrals can be greatly simplified based on such properties. For the symmetric loading condition with  $c_1 = c_3 = 0$ , one can write

$$\varepsilon_{11}^{*} = -x_{1}^{-\lambda} \frac{(\lambda - 1) \left(c_{2}(\lambda - 2)\cos \lambda\theta + c_{4}(2\cos \lambda\theta + \lambda\cos(\lambda + 2)\theta)\right)}{2\mu^{1}} \\
\varepsilon_{12}^{*} = -x_{1}^{-\lambda} \frac{(\lambda - 1) \left(c_{2}(\lambda - 2)\sin \lambda\theta + c_{4}\lambda\sin(\lambda + 2)\theta\right)}{2\mu^{1}} \\
\varepsilon_{22}^{*} = x_{1}^{-\lambda} \frac{(\lambda - 1) \left(c_{4}\lambda\cos(\lambda + 2)\theta + \left(c_{2}(\lambda - 2) - 2c_{4}\right)\cos \lambda\theta\right)}{2\mu^{1}}$$
(35)

and domain integrals can be simplified as

$$\int_{\Omega^{P}} s_{11kl} \varepsilon_{kl}^{*} d\mathbf{x}' = x_{1}^{-\lambda} \frac{(\lambda - 1) \csc \lambda \pi}{16\mu^{1} (1 - v^{0})} \left\{ 2c_{2}(\lambda - 2) \left[ -(\lambda - 1) \sin[\lambda \pi + 2\beta(2 - \lambda)] + (\lambda - 4v^{0} + 2) \sin[\lambda \pi + 2\beta(1 - \lambda)] + (4v^{0} - 3) \sin \lambda \pi \right] + 2c_{4} \left[ (2 - (\lambda - 2)\lambda) \sin[\lambda \pi + 2\beta(1 - \lambda)] + (\lambda - 1) \left( (\lambda - 4v^{0} + 2) \sin \lambda(\pi - 2\beta) - 2 \sin[\lambda \pi + 2\beta] \right) + \sin \lambda \pi \left[ -\lambda + 4(\lambda - 1)v^{0} - 2 \right] \right] \right\}$$
(36)

and

$$\int_{\Omega^{P}} s_{22kl} \varepsilon_{kl}^{*} d\mathbf{x}' = -x_{1}^{-\lambda} \frac{(\lambda - 1) \csc \lambda \pi}{16\mu^{1}(1 - v^{0})} \left\{ 2c_{2}(\lambda - 2) \left[ (1 - \lambda) \sin[\lambda \pi + 2\beta(2 - \lambda)] + (\lambda + 4v^{0} - 2) \sin[\lambda \pi + 2\beta(1 - \lambda)] + (1 - 4v^{0}) \sin \lambda \pi \right] + c_{4} \left[ 4(1 - \lambda) \sin[\lambda \pi + 2\beta] + 2(\lambda - 1)(\lambda + 4v^{0} - 2) \sin \lambda(\pi - 2\beta) + 4 \left[ (\lambda - 2)\lambda - 2 \right] \sin \lambda \pi \left[ -3\lambda + 4(\lambda - 1)v^{0} + 6 \right] \sin[\lambda \pi + 2\beta(1 - \lambda)] \right] \right\}$$
(37)

Combining contribution from  $S^d_{ijkl} \epsilon^{\epsilon}_{kl}(0^+,0)$ , one can obtain a linear equation system on stress equivalence for the 11 and 22 components by substituting Eqs. (36) and (37) into (34), and two equations can be acquired by ignoring  $r^{-\lambda}$  and partial differentiation with respect to  $\lambda$  as follows:

$$-\frac{(\lambda - 1)\csc \lambda \pi}{8\mu^{1}(1 - v^{0})} \left\{ c_{4} \left[ [(\lambda - 2)\lambda - 2]\sin[\lambda \pi + 2\beta(1 - \lambda)] + (\lambda - 1)(2\sin[\lambda \pi + 2\beta] - (\lambda - 4v^{0} + 2)\sin\lambda(\pi - 2\beta)) \right. \right.$$

$$-3\sin \lambda \pi (\lambda - 4v^{0} + 2) \left] -c_{2}(\lambda - 2) \left[ (1 - \lambda)\sin[\lambda \pi + 2\beta(2 - \lambda)] + \sin\lambda \pi + (\lambda - 4v^{0} + 2)\sin[\lambda \pi + 2\beta(1 - \lambda)] \right] \right\} = 0$$

$$-\frac{(\lambda - 1)\csc(\pi \lambda)}{8\mu^{1}(1 - v^{0})} \left\{ c_{2}(\lambda - 2) \left[ -(\lambda - 1)\sin[\lambda \pi + 2\beta(2 - \lambda)] + \sin\lambda \pi + (\lambda + 4v^{0} - 2)\sin[\lambda \pi + 2\beta(1 - \lambda)] \right] \right.$$

$$+ c_{4} \left[ [2 - (\lambda - 2)\lambda]\sin[\lambda \pi + 2\beta(1 - \lambda)] + (\lambda - 1)((\lambda + 4v^{0} - 2)\sin\lambda(\pi - 2\beta) - 2\sin[\lambda \pi + 2\beta]) \right.$$

$$+ 3\sin\lambda \pi (\lambda + 4v^{0} - 2) \right] \right\} = 0$$

$$(38)$$

Notice that to find a nontrivial solution to such a system, the determinant of the  $2 \times 2$  coefficient matrix should be zero, also known as the eigenvalue problem. With a lengthy but straightforward derivation, the determinant of coefficient matrix of  $c_2$  and  $c_4$  can be obtained (ignoring  $x_1$ ):

$$-\frac{(\lambda-2)(\lambda-1)^2(1-2v^0)\csc^2(\lambda\pi)}{32(\mu^1)^2(1-v^0)^2} \left\{ (\lambda-1)^2(\cos 4\beta-1) + 3(\lambda-1)[\cos 2(\lambda-2)\beta - \cos 2\lambda\beta] - (\lambda+2)\cos[2\lambda\pi+2\beta(2-\lambda)] + (\lambda-1)\cos[2\lambda(\pi-\beta)] + 3\cos 2\lambda\pi \right\} = 0$$
(40)

Therefore, a list of roots of  $\lambda$  can be obtained.

For anti-symmetric loading problem with  $c_2 = c_4 = 0$ , the eigenstrain can be written as,

$$\varepsilon_{11}^{*} = x_{1}^{-\lambda} \frac{(\lambda - 1) \left( c_{1}(\lambda - 2) \sin \lambda \beta - c_{3}(2 \sin \lambda \beta + \lambda \sin(\lambda + 2)\beta) \right)}{2\mu^{1}} \\
\varepsilon_{12}^{*} = x_{1}^{-\lambda} \frac{(\lambda - 1) \left( c_{3}\lambda \cos(\lambda + 2)\beta - c_{1}(\lambda - 2) \cos \lambda \beta \right)}{2\mu^{1}} \\
\varepsilon_{22}^{*} = -x_{1}^{-\lambda} \frac{(\lambda - 1) \left( c_{1}(\lambda - 2) \sin \lambda \beta + c_{3}(2 \sin \lambda \beta - \lambda \sin(\lambda + 2)\beta) \right)}{2\mu^{1}}$$
(41)

and domain integrals can be simplified as,

$$\int_{\Omega^{\rho}} s_{12kl} \varepsilon_{kl}^* d\mathbf{x}' = -|x_1|^{-\lambda} \frac{(\lambda - 1) \csc \lambda \pi}{16\mu^1 (1 - v^0)} \left\{ 2c_3 \left[ -(\lambda - 1) \left[ \lambda \sin \lambda (\pi - 2\beta) + 2\sin(\lambda \pi + 2\beta) \right] + \left[ (\lambda - 2)\lambda - 2 \right] \sin[\lambda \pi + 2\beta(1 - \lambda)] + 3\lambda \sin \lambda \pi \right] - 2c_1(\lambda - 2) \left[ -\sin[\lambda \pi + 2\beta(2 - \lambda)] + 2\lambda \sin \beta \cos[\lambda \pi + \beta(3 - 2\lambda)] + \sin \lambda \pi \right] \right\}$$

$$(42)$$

Based on the expansion of Airy's stress function, for shearing problems, the number of unknown coefficients is two except for the singularity parameter. However, Eq. (42) only provides one equation to solve two unknowns. Eshelby's equivalent inclusion method mathematically transforms the BVP into the superposition of two BVPs through the stress equivalent condition (Yin et al., 2022), which can be transferred in form of the displacement gradients of  $u_{i,j}$ . The stress equivalence of  $(\sigma_{12})$  combines two independent displacement gradients of  $u_{1,2}$  and  $u_{2,1}$ , through which the symmetric part of  $\frac{1}{2}(u_{1,2}+u_{2,1})$  is taken into consideration in Eq. (42). Due to the symmetry of stress and strain, either  $u_{1,2}$  or  $u_{2,1}$  at the same value will produce the same stress of  $\sigma_{12}$ , which is insensitive to the rotational component of  $u_{1,2}-u_{2,1}$ . However, in this problem, because the rotational component on inhomogeneity will affect the interfacial continuity, so that the stress equivalence needs to be set up on  $u_{1,2}$  and  $u_{2,1}$ , respectively, which will automatically make stress equivalence of  $\sigma_{12}$  satisfied. For example,

$$u_{2,1}' = \int_{\Omega^p} g_{2kl,1} \varepsilon_{kl}^* d\mathbf{x}' = -|x_1|^{-\lambda} \frac{(\lambda - 1)\csc \lambda \pi}{16\mu^1 (1 - v^0)} \left\{ 2c_1(\lambda - 2) \left[ -(\lambda - 1)\sin[\lambda \pi + 2\beta(2 - \lambda)] + (\lambda + 4v^0 - 4)\sin[\lambda \pi + 2\beta(1 - \lambda)] + (3 - 4v^0)\sin \lambda \pi \right] + 2c_3 \left[ [(\lambda - 2)\lambda - 2]\sin[\lambda \pi + 2\beta(1 - \lambda)] + (\lambda - 1) \left( -2\sin[\lambda \pi + 2\beta] - \left( (\lambda + 4v^0 - 4)\sin \lambda(\pi - 2\beta) \right) \right) + \sin \lambda \pi [-\lambda + 4(\lambda - 1)v^0 + 4] \right] \right\}$$

$$(43)$$

where the actual derivative of displacement  $u_{2,1}$  can be obtained through Airy's stress function as,

$$u_{2,1} = x_1^{-\lambda} \frac{(\lambda - 1) \left( c_3(\lambda - 4) - c_1(\lambda - 2) \right)}{2u^1} \tag{44}$$

Note that in a specific boundary value problem for an inhomogeneity under a uniform far field stress, the stress equivalent condition shall be set up at each order of  $\lambda$  to solve for  $c_i$  (i=1,2,3,4). When  $\lambda=0$ , a uniform displacement gradient  $u_{i,j}^0$ =constant shall be included in  $u_{2,1}'+u_{2,1}^0=u_{2,1}$ . For any case  $\lambda\neq0$ , the displacement gradient beyond the constant term shall satisfy  $u_{2,1}'=u_{2,1}$  in the above two equations. Similarly, the same procedure can be applied to  $u_{1,2}$ . Therefore, one can obtain the equation system of  $c_1$  and  $c_3$  by ignoring  $r^{-\lambda}$  and partial differentiation with respect to  $\lambda$  as follows:

$$\frac{(1-\lambda)\csc{\lambda\pi}}{8\mu^{1}(1-v^{0})} \left\{ c_{3} \left[ -(\lambda-1)\left(\lambda\sin{\lambda(\pi-2\beta)} + 2\sin[\lambda\pi+2\beta]\right) + (\lambda^{2}-2\lambda-2)\sin[\lambda\pi+2\beta(1-\lambda)] + 3\lambda\sin{\lambda\pi} \right] \right.$$

$$\left. - c_{1}(\lambda-2) \left[ -\sin[\lambda\pi+2\beta(2-\lambda)] + 2\lambda\sin{\beta}\cos[\lambda\pi+\beta(3-2\lambda)] + \sin{\lambda\pi} \right] \right\} = 0$$

$$\frac{(\lambda-1)\csc{\lambda\pi}}{16\mu^{1}(1-v^{0})} \left\{ c_{3} \left[ (2-\lambda^{2}+2\lambda)\sin[\lambda\pi+2\beta(1-\lambda)] + (\lambda-1)\left(2\sin[\lambda\pi+2\beta] + (\lambda-4v^{0}+4)\sin{\lambda(\pi-2\beta)}\right) + 3\sin{\lambda\pi}(-\lambda+4v^{0}-4) \right] + c_{1}(\lambda-2) \left[ (\lambda-1)\sin[\lambda\pi+2\beta(2-\lambda)] + \sin{\lambda\pi} + (-\lambda+4v^{0}-4)\sin[\lambda\pi+2\beta(1-\lambda)] \right] \right\} = 0$$

$$(45)$$

Similarly to the symmetric case, the determinant of the coefficient matrix shall be zero, to assure a nontrivial solution of  $c_1$  and  $c_3$ , as follows:

$$\frac{(\lambda - 2)(\lambda - 1)^2 \csc^2 \lambda \pi}{64(\mu^1)^2 (1 - v^0)} \left\{ (\lambda - 1)^2 (\cos 4\beta - 1) - (\lambda - 1) \left[ 3\cos 2(\lambda - 2)\beta + \cos 2\lambda(\pi - \beta) - 3\cos 2\lambda\beta - \cos(2\lambda\pi - 2\beta\lambda + 4\beta) \right] - 3\cos[2\lambda\pi + 4\beta(1 - \lambda)] + 3\cos(2\lambda\pi) \right\} = 0$$
(47)

which can provide a list of roots of  $\lambda$ .

# 3.2. Slit-like crack problem

When  $\beta \to 0$ , the above problem with a triangular void is reduced to the classic slit-like crack problem, which shows  $1/\sqrt{r}$  singular distribution of strain fields around the crack tip. Unlike the conventional method of adjusting ratios of ellipsoids (Mura, 1987), this section directly uses a triangular void. Before solving Eq. (40), recall the classic work of slit-like crack from Refs. (Mura,

1987; Bulatov and Cai, 2006), which applies Griffith's criteria and Eshelby's equivalent inclusion method, respectively. On the other hand, because the Eshelby's tensor of ellipsoid for the interior point is uniform, thus eigenstrain must be uniform when the crack is simulated using an adjusted ellipsoid (Bulatov and Cai, 2006). For Mode I of opening-mode cracking problem subjected to  $\sigma_{22}^0$  in the far field, eigenstrain can be obtained as  $\varepsilon_{11}^*$  is finite while  $\varepsilon_{22}^* = A\varepsilon_{11}^*$ , where A is ratio of two axis  $a_1/a_2$  ( $a_2 \to 0$ ). Based on Eshelby's tensor for exterior points, stress around the crack tip exhibits  $1/\sqrt{r}$  singular distribution. On the other hand, for any arbitrary opening angles, such a uniform eigenstrain will only generate  $\ln r$  singular distribution for triangular tips (Rodin, 1996). Therefore, the solution is not applicable for triangular inhomogeneities, even for slit-like cracks simulated by triangular inhomogeneities. The present formulation provides a consistent explanation to Mode I and Mode II fracture analysis as follows:

# 3.2.1. Mode I: uni-axial loading $\sigma_{22}^0$

Consider the material with a crack under the far field stress of  $\sigma_{22}^0$ . The equivalent stress condition for the voids is written  $\varepsilon_{kl}^0 + \varepsilon_{kl}' - \varepsilon_{kl}^* = (C_{iikl}^0)^{-1} \sigma_{ij} = 0$ . Under the symmetric load case of the plane strain problem, one can write,

$$-\frac{v^0}{2\mu^0}\sigma_{22}^0 + \epsilon_{11}' - \epsilon_{11}^* = 0 \tag{48a}$$

$$\frac{1 - v^0}{2u^0} \sigma_{22}^0 + \varepsilon_{22}' - \varepsilon_{22}^* = 0 \tag{48b}$$

where  $-\frac{v^0}{2\mu^0}\sigma_{22}^0 = \varepsilon_{11}^0$  and  $\frac{1-v^0}{2\mu^0}\sigma_{22}^0 = \varepsilon_{22}^0$  are used under the far-field load of  $\sigma_{22}^0$ . Note that Eq. (48) leads to a series solution, which may contain many terms with different power distributions of  $\lambda$ . However, only  $\lambda \in [0,1)$  is of interest for the singularity. When  $\beta \to 0$ ,  $\sin \beta \approx \beta + \mathcal{O}(\beta)$ , which can be utilized to simplify equivalent stress conditions of  $\sigma_{11}$  and  $\sigma_{22}$ . Using the determinant of coefficient matrix Eq. (40), one can determine the highest singular parameter  $\lambda$  that,

$$Det = \frac{(1 - 2v^0)(\lambda - 2)(\lambda - 1)^3}{2(\mu^1)^2(1 - v^0)^2} \cot \lambda \pi \left\{ \beta - 2(\lambda - 1)\cot(\lambda \pi)\beta^2 \right\} + \mathcal{O}(\beta^3)$$
(49)

where the determinant is written as series approximation when  $\beta \to 0^+$ . In the range of  $\lambda < 1$  (Barber, 1992),  $\lambda = (-i + 1/2)\pi$  with i = 0, 1, 2, ..., which enables nontrivial solutions for the boundary value problem. Therefore, the singularity parameter of  $\lambda$  is 1/2 corresponding to i = 0, and all other cases for i = 1, 2, ... exhibit no singularity.

# 3.2.2. Mode II: simple shearing $\sigma_{12}^0$

Consider the material with a crack under the far field stress of  $\sigma_{12}^0 = 2\mu^0(u_{1,2}^0 + u_{2,1}^0)$ . The equivalent stress condition for the voids is written  $\varepsilon_{kl}^0 + \varepsilon_{kl}' - \varepsilon_{kl}^* = (C_{ijkl}^0)^{-1}\sigma_{ij} = 0$ . Under the antisymmetric load case, one can write,

$$\frac{\sigma_{12}^0}{2\mu^0} + \epsilon_{12}' - \epsilon_{12}^* = 0 \tag{50a}$$

$$u_{1,2}^0 + u_{1,2}' - u_{1,2} = 0$$
 or  $u_{2,1}^0 + u_{2,1}' - u_{2,1} = 0$  (50b)

Following the same fashion as the last subsection, the determinant in Eq. (47) can be simplified as,

$$Det = \frac{(\lambda - 2)\cot \lambda \pi}{2(\mu^1)^2 (1 - \nu^0)} \left\{ (1 - \lambda)^3 \beta + 4 \frac{(\lambda - 1)^4}{(1 - \nu^0)} \beta^2 \right\} + \mathcal{O}(\beta^3) = 0$$
 (51)

where the singularity parameter of  $\lambda = \frac{1}{2}$  in the range of  $\lambda \in (0, 1)$ .

The dominant singularity of the two modes is the same as the classic solution of  $1/\sqrt{r}$ . Therefore, for a triangular void with  $\beta \to 0$ , it reduces to a slit-like crack, and both the stress and the eigenstrain fields around the tip exhibit a dominant singularity at  $1/\sqrt{r}$ .

# 3.3. General triangular void problems

Williams (1952) and Dempsey and Sinclair (1979) investigated the singularity of angular wedge and composites wedge, respectively. As demonstrated in the previous subsection, the solution to the eigenstrain contains a series of components with different  $\lambda$ . However, the dominant singularity is of our most interest. Therefore, this section aims to use Eshelby's equivalent inclusion method to solve dominant stress singularities, which serves as both a verification and tribute to pioneers' classic works. Solving Eq. (40) with angles varying  $\beta \in [0, \pi/2]$ , the dominant stress singularities are plotted in Fig. 3, which shows that the singularity parameter  $\lambda$  solved by EIM is exactly the same as Williams' classic solution for the symmetric case. Similarly, the anti-symmetric case by obtained by solving Eq. (47).

In Fig. 3, for Mode I of the symmetric case, the singularity parameter  $\lambda$  gradually reduce from 0.5 to 0 when  $\beta$  increases from 0 to  $\frac{\pi}{2}$ . However, for Mode II of the anti-symmetric case, the singularity parameter become zero when  $\beta=0.285\pi$  or  $51.3^{\circ}$ . The reduction of  $\lambda$  with  $\beta$  for Mode II is much faster than that for Mode I. The Eshelby's EIM solution reproduces Williams' solution (Williams, 1952; Barber, 1992).

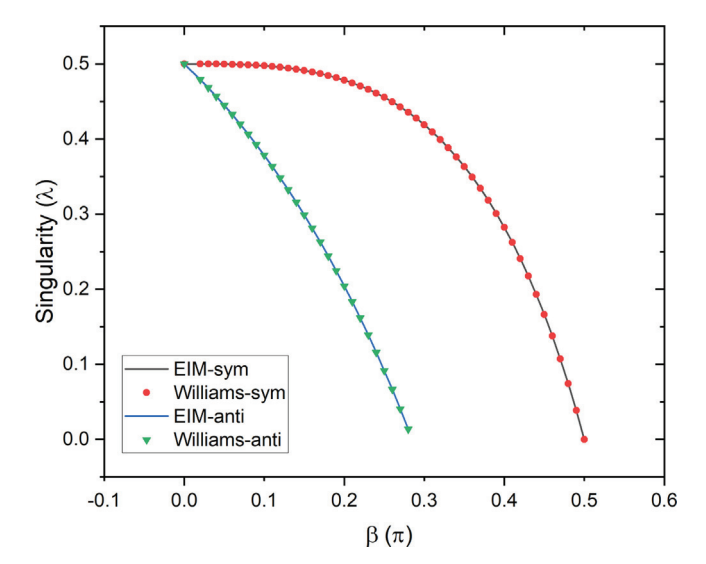


Fig. 3. Comparison of symmetric and anti-symmetric dominant singularity of a triangular void by EIM with Williams' solution of the re-entrant corner.

## 4. General triangular inhomogeneity problems

In the preceding section, EIM was applied to identify the dominant singularity of triangular void problems, and it agrees well with the classic solutions. Voids are special inhomogeneities with zero stiffness tensor and zero stress; while general inhomogeneities may exhibit nonzero but different material properties than the matrix, which leads to a stress field in the inhomogeneity as well. As explained in Section 2.3, to extend the power function distribution to the logarithmic singularity of  $r^{-\lambda} \ln r$ , a partial derivative with respect to singularity parameter  $\lambda$  was introduced by Dempsey and Sinclair (1979). Dundurs (1969) and Bogy (1968) have investigated that the logarithmic singularity can be sufficiently determined by two material constants, namely  $\alpha$  and  $\beta$  in their works. This section will investigate the eigenstrain distribution or stress discontinuities around the vertex for inhomogeneities, particularly with logarithm singularities. The present formulation provides a systemic way to investigate the singularity and discontinuities of stress around the vertex of inhomogeneities.

## 4.1. About the logarithmic singularity of inhomogeneity problems

Following Dempsey and Sinclair (1981), when the derivative of the determinant of the EIM equations on  $\lambda$  is zero, a logarithmic singularity appears, and the solution scheme for inhomogeneities can be revised from the previous procedure as follows:

- 1. Apply power function distribution in the same fashion as the triangular voids, and construct two independent integral equations for symmetric or anti-symmetric problems, respectively.
- 2. Non-trivial solutions can be obtained by setting determinant of the matrix as zero, which is more complicated than the triangular void because the stiffness of the inhomogeneity is not zero anymore. The singularity parameter  $\lambda$  can be solved similarly.
- 3. Check if the derivative of the determinant on  $\lambda$  is zero. If it is zero, the singularity level of the stress and eigenstrain is  $r^{-\lambda} \ln r$ ; otherwise, it still follows  $r^{-\lambda}$ , the same as the last section (Dempsey and Sinclair, 1979).

In the following, the symmetric and anti-symmetric cases will be studied with the formulation for the general inhomogeneity problem. Parametric studies are conducted on the ratio of shear modulus  $\mu^0/\mu^1$  and opening angle  $\beta$ .

Note that Section 3 provides analysis on the void problems, which exhibits zero shear modulus on the inhomogeneity. As a consequence, equivalent stress conditions can be greatly simplified as equivalence between disturbed strain and eigenstrain for singularity identification. The authors have checked the determinant and its partial derivative cannot be zero at the same time for voids, and such a procedure is illustrated in the supplementary information with scripts.

In addition, Dundurs (1969) commented on Bogy's work (Bogy, 1968), and mentioned that singular behaviors are dependent on two parameters. We can use the two parameters to determine the existence of the logarithmic singularity as well, which will be discussed in Section 4.4. Dempsey and Sinclair's method (Dempsey and Sinclair, 1979) provides the consistent prediction of the logarithmic singularity as Dundurs (1969) for the wedge problem of bi-material systems. The inhomogeneity problem in this paper can follow the same way (Dempsey and Sinclair, 1979). In the following, the derivative of the determinant on  $\lambda$  will also be evaluated for all cases of the two parameters, but in most cases no such solution exists to make both the determinant and the derivative of the determinant equal to zero, which means that the logarithmic singularity does not exist for the singularity problem of most cases. However, special cases do exist for the logarithmic singularity.

(55)

# 4.2. Mode I: uni-axial loading $\sigma_{22}^0$

Based on the equivalent stress conditions, two equations can be obtained as,

$$\begin{split} &\frac{(1-\lambda)}{8\mu^0\mu^1(1-v^0)} \left\{ \ c_2(\lambda-2) \left[ \ -\mu^0 - 3\mu^1 + \csc\lambda\pi(\mu^0 - \mu^1) \Big( (\lambda-1)\sin[\lambda\pi + 2\beta(2-\lambda)] + (-\lambda + 4v^0 - 2)\sin[\lambda\pi + 2\beta(1-\lambda)] \right) \right. \\ &+ 4\mu^1v^0 \left] + c_4\csc\lambda\pi \left[ \ (\lambda-1) \Big( 2\sin[\lambda\pi + 2\beta][\mu^0(1-2v^1) - \mu^1(1-2v^0)] - (\mu^0 - \mu^1)(\lambda - 4v^0 + 2)\sin\lambda(\pi - 2\beta) \Big) \right. \\ &+ \sin[\lambda\pi + 2\beta(1-\lambda)] \Big( \mu^0[(\lambda-2)\lambda + 4v^1 - 2] - \mu^1[(\lambda-2)\lambda + 4v^0 - 2] \Big) + \Big( \sin\lambda\pi(-\lambda + 4v^0 - 2)((3-4v^1)\mu^0 + \mu^1) \Big) \right] \Big\} = 0 \\ &\frac{(1-\lambda)}{8\mu^0\mu^1(1-v^0)} \left\{ \ c_2(\lambda-2) \left[ \ \mu^0 + 3\mu^1 + \csc\lambda\pi(\mu^0 - \mu^1) \Big( (\lambda + 4v^0 - 2)\sin[\lambda\pi + 2\beta(1-\lambda)] - (\lambda-1)\sin[\lambda\pi + 2\beta(2-\lambda)] \Big) \right. \\ &- 4\mu^1v^0 \right] + c_4\csc\lambda\pi \left[ \ (\lambda-1) \Big( (\mu^0 - \mu^1)(\lambda + 4v^0 - 2)\sin\lambda(\pi - 2\beta) - 2\sin[\lambda\pi + 2\beta] \left[ \mu^0(1-2v^1) - \mu^1(1-2v^0) \right] \Big) \right. \\ &+ \sin[\lambda\pi + 2\beta(1-\lambda)](\mu^1[(\lambda-2)\lambda + 4v^0 - 2] - \mu^0[(\lambda-2)\lambda + 4v^1 - 2)] + \Big( \sin\lambda\pi(\lambda + 4v^0 - 2)((3-4v^1)\mu^0 + \mu^1) \Big) \right] \Big\} = 0 \end{split}$$

and the determinant of the coefficients of the two equations is,

$$\begin{split} & \operatorname{Det}_{n} = \frac{(2-\lambda)(\lambda-1)^{2}(1-2v^{0}) \csc \lambda \pi}{16(\mu^{0}\mu^{1})^{2}(1-v^{0})^{2}} \; \left\{ \; (\mu^{0}-\mu^{1}) \left[ \; (\lambda-1) \sin \lambda(\pi-2\beta) \left( \; (\lambda-1) \csc \lambda \pi (\mu^{0}-\mu^{1}) \sin[\lambda\pi+2\beta(2-\lambda)] \right. \right. \right. \\ & \left. - \mu^{0} - (3-4v^{0})\mu^{1} \; \right) + \csc \lambda \pi \sin[\lambda\pi+2\beta(1-\lambda)] \left( \; -2(\lambda-1) \sin[\lambda\pi+2\beta][\mu^{0}(1-2v^{1})-\mu^{1}(1-2v^{0})] \right. \\ & \left. + \sin[\lambda\pi+2\beta(1-\lambda)] \left[ \mu^{1} \left( (\lambda-2)\lambda+4v^{0}-2 \right) - \mu^{0} \left( (\lambda-2)\lambda+4v^{1}-2 \right) \right] \; \right) - (1-\lambda) \sin[\lambda\pi+2\beta(2-\lambda)][(3-4v^{1})\mu^{0}+\mu^{1}] \right] \\ & \left. - \sin \lambda \pi [\mu^{0}+\mu^{1}(3-4v^{0})](\mu^{0}(3-4v^{1})+\mu^{1}) \; \right\} = 0 \end{split}$$

Similarly, one can solve for  $\lambda$  and obtain the singularity order. To check if the logarithmic singularity exists, one can take the first order partial derivative of Det, with respect to  $\lambda$  as,

When  $\operatorname{Det}_n = 0$  is applied to determine the singularity parameter  $\lambda$ , one can substitute  $\lambda$  into the above equation. If  $\frac{\partial \operatorname{Det}_n}{\partial \lambda} = 0$ , the singularity level will be  $r^{-\lambda} \ln r$ ; otherwise, it is  $r^{-\lambda}$ .

To show numerical results on dominant singularities, consider properties as  $\mu^0=1, v^0=v^1=\frac{1}{4}$ . Fig. 4(a) plots  $\lambda$  changing with the shear modulus ratio  $\mu^1/\mu^0$  for five cases of  $\beta$ . When  $\mu^1=\mu^0$ , stress singularity does not exist because of no material mismatch. The curve " $\beta=0$ " in Fig. 4(a) shows that singularity  $\lambda$  decreases rapidly with increase of  $\mu^1$ . Even if  $\mu^1=0.1\mu^0$ ,  $\lambda$  rapidly decreases from  $\frac{1}{2}$  to < 0.15; when  $\mu^1$  is greater than  $\mu^0$  along with the increase of material mismatch, the singularity parameter  $\lambda$  gradually increases to 1/2, which is not explicitly shown in the log scale coordinate. In the most range of  $\mu^1/\mu^0$ , the singularity parameter of the curve " $\beta=0$ " is smaller than the other four cases except  $\mu^1/\mu^0=0$  or  $\infty$ . When  $\beta$  increases, the singularity parameter varies in a smaller range.

Fig. 4(b) shows the singularity parameter changing with  $\beta$  for six cases of  $\mu^1/\mu^0$ . When  $\mu^1/\mu^0=0$ ,  $\lambda$  decreases slowly when  $\beta$  is small, and the changing rate increases rapidly when  $\beta$  approaches  $0.5\pi$ , which implies that  $\lambda$  is highly sensitive to both material mismatch and opening angles. For two extreme cases of material mismatch ( $\mu^1/\mu^0=0$  or  $\infty$ ),  $\lambda$  can be described by a monotonic function of the opening angle  $\beta$ , and the maximum values exist when  $\beta \to 0^+$ . When  $\mu^1/\mu^0 < 1$ , the maximum value exists in the second half ( $\beta > 0.25\pi$ ) and the curve becomes more flatten for smaller material mismatch; when  $\mu^1/\mu^0 > 1$ , the maximum value exists in the first half ( $\beta < 0.25\pi$ ) and the shape of curve depends on material mismatch as well. It is observed that when  $\beta \to 0$ ,  $\lambda$  of four cases  $0.1 \le \mu^1/\mu^0 \le 10$  are not  $\frac{1}{2}$ , which differentiates from the slit-like crack problem.

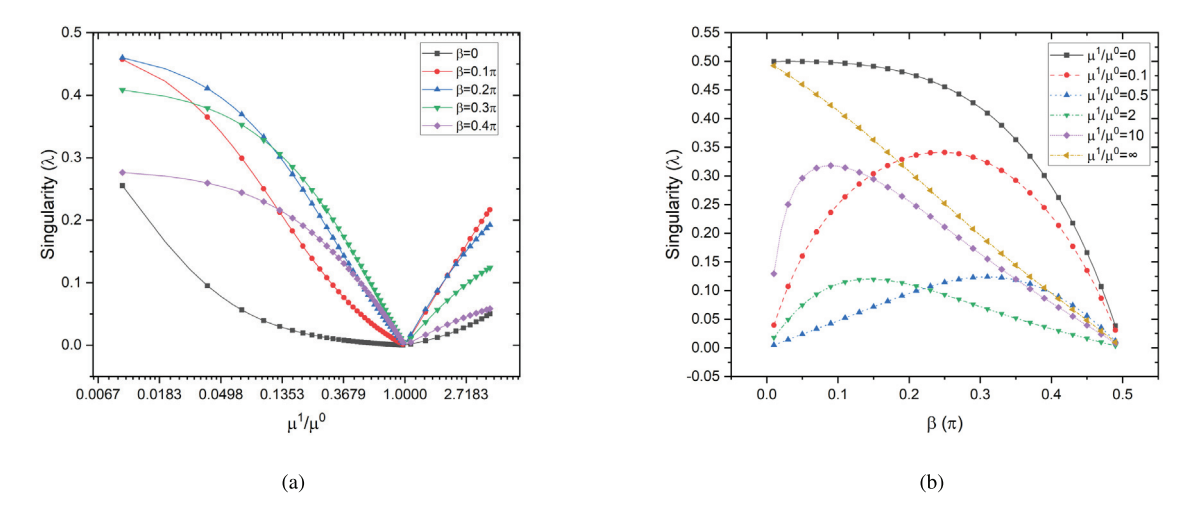


Fig. 4. Variation of symmetric dominant stress singularity  $\lambda$ , (a) opening angle  $\beta = 0, 0.10, 0.2, 0.3$  and  $0.4\pi$  with ratio of shear modulus  $\mu^1/\mu^0 \in [0.001, 4]$ ; (b) ratio of shear modulus  $\mu^1/\mu^0 = 0, 0.1, 0.5, 2, 10$  and  $\infty$  versus opening angle  $\beta \in [0, 1/2)\pi$ .

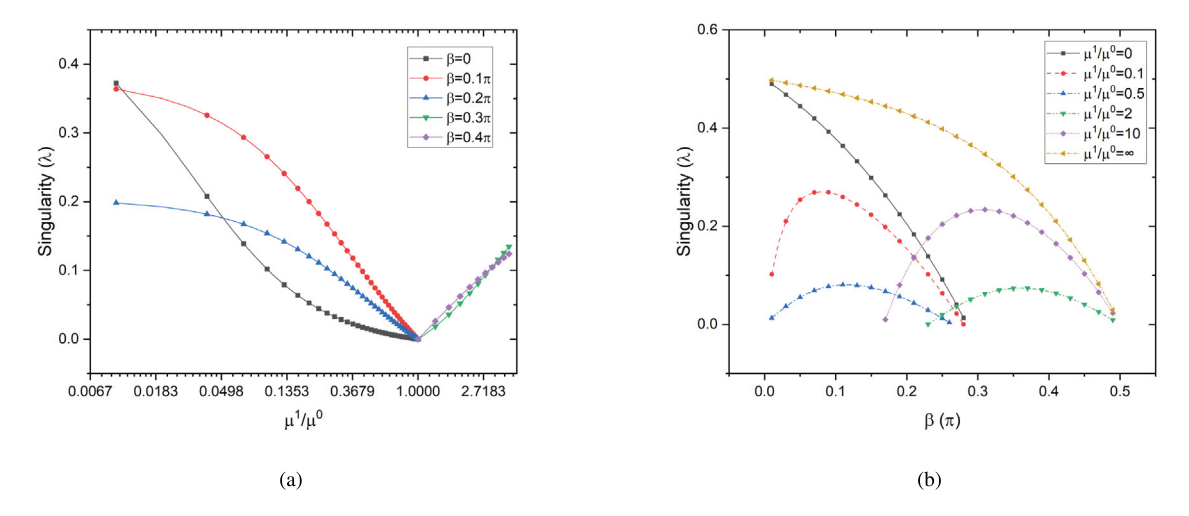


Fig. 5. Variation of anti-symmetric dominant stress singularity  $\lambda$ , (a) opening angle  $\beta = 0, 0.10, 0.2, 0.3$  and  $0.4\pi$  with ratio of shear modulus  $\mu^1/\mu^0 \in [0.001, 4]$ ; (b) ratio of shear modulus  $\mu^1/\mu^0 = 0, 0.1, 0.5, 2, 10$  and  $\infty$  versus opening angle  $\beta \in [0, 1/2)\pi$ .

# 4.3. Mode II: simple shearing $\sigma_{12}^0$

Based on equivalent stress conditions, two equations can be obtained,

$$\frac{(1-\lambda)}{8\mu^{0}\mu^{1}(1-v^{0})} \left\{ c_{3} \csc \lambda \pi \left[ (\lambda-1) \left( \lambda(\mu^{1}-\mu^{0}) \sin \lambda(\pi-2\beta) - 2 \sin[\lambda\pi+2\beta][\mu^{0}(1-2v^{1}) - \mu^{1}(1-2v^{0})] \right) \right. \right.$$

$$+ \sin[\lambda\pi+2\beta(1-\lambda)] \left( \mu^{0}[(\lambda-2)\lambda+4v^{1}-2] - \mu^{1}[(\lambda-2)\lambda+4v^{0}-2] \right) + \lambda \sin(\pi\lambda)(3\mu+\mu^{1}-4\mu v^{1}) \left. \right]$$

$$- c_{1}(\lambda-2) \left[ \csc \lambda \pi(\mu^{0}-\mu^{1}) \left( 2\lambda \sin \beta \cos[\lambda\pi+(3-2\lambda)\beta] - \sin[\lambda\pi+2\beta(2-\lambda)] \right) + \mu^{0}+\mu^{1}(3-4v^{0}) \right] \right\} = 0$$

$$\frac{(1-\lambda)}{8\mu^{0}\mu^{1}(1-v^{0})} \left\{ c_{1}(\lambda-2) \left[ -\mu^{0}-3\mu^{1}+\csc \lambda\pi(\mu^{0}-\mu^{1}) \left( (\lambda+4v^{0}-4)\sin[\lambda\pi+2\beta(1-\lambda)] - (\lambda-1)\sin[\lambda\pi+2\beta(2-\lambda)] \right) \right.$$

$$+ 4\mu^{1}v^{0} \right] + c_{3} \csc \lambda\pi \left[ (\lambda-1) \left( -2\sin[\lambda\pi+2\beta][\mu^{0}(1-2v^{1}) - \mu^{1}(1-2v^{0})] - (\mu^{0}-\mu^{1})(\lambda+4v^{0}-4)\sin \lambda(\pi-2\beta) \right)$$

$$+ \sin[\lambda\pi+2\beta(1-\lambda)] \left( \mu^{0}((\lambda-2)\lambda+4v^{1}-2) - \mu^{1}[(\lambda-2)\lambda+4v^{0}-2] \right) + \left( \sin \lambda\pi(\lambda+4v^{0}-4)((3-4v^{1})\mu^{0}+\mu^{1}) \right) \right] \right\} = 0$$

and the determinant of the coefficients of the two equations is,

$$\begin{aligned} & \operatorname{Det}_{s} = \frac{(2-\lambda)(\lambda-1)^{2}}{16(\mu^{0}\mu^{1})^{2}(1-v^{0})} \left\{ \csc^{2}\lambda\pi(\mu^{0}-\mu^{1})\sin[\lambda\pi+2\beta(1-\lambda)] \left[ (\lambda-1)\left(\lambda(\mu^{1}-\mu^{0})\sin\lambda(\pi-2\beta)-2\sin[\lambda\pi+2\beta] \right] \right. \\ & \left. \left[ \mu^{0}(1-2v^{1})-\mu^{1}(1-2v^{0}) \right] \right. \right. \\ & \left. \left. \left. \left( +\sin\lambda\pi(\mu^{0}-\mu^{1})\sin(\lambda\pi+2\beta(1-\lambda)) \right) \left( \mu^{0}[(\lambda-2)\lambda+4v^{1}-2]-\mu^{1}[(\lambda-2)\lambda+4v^{0}-2] \right) \right. \\ & \left. \left. \left( +\lambda\sin\lambda\pi[\mu^{1}+\mu(3-4v^{1})] \right] - \left[ (\lambda-1)\csc\lambda\pi(\mu^{0}-\mu^{1})\sin\lambda(\pi-2\beta)-\mu^{1}-\mu^{0}(3-4v^{1}) \right] \left[ \csc\lambda\pi(\mu^{0}-\mu^{1}) \right. \\ & \left. \left( 2\lambda\sin\beta\cos[\pi\lambda+\beta(3-2\lambda)] - \sin[\lambda\pi+2\beta(2-\lambda)] \right) + \mu^{0} + \mu^{1}(3-4v^{0}) \right. \right] \right\} = 0 \end{aligned}$$

Taking the first order partial derivative with respect to  $\lambda$ , one can obtain:

Similarly to Fig. 4(a), Fig. 5(a) plots  $\lambda$  changing with  $\mu^1/\mu^0$  for the shearing case. As shown in Fig. 3, a singularity for the shearing case does not exist for a re-entrant corner for all angles. For example, when  $\beta=0.1\pi$ , singularity exists for ratio of shear modulus  $\mu^1/\mu^0\in(0,1)$ ; when  $\beta=0.4\pi$ , singularity exists for ratio of shear modulus  $\mu^1/\mu^0\in(1,\infty)$  instead. The singularity may exist at larger opening angles for stiffer inhomogeneities. Similar trends of singularity can be observed that it increases with larger material differences, no matter for softer or stiffer inhomogeneities.

Fig. 5(b) plots singularity versus opening angles. The shape of curves is similar to symmetric loading cases, and their main difference lies in the existing range of angles. Notice that the determination of singularity  $\lambda$  is independent of logarithm singularity. To investigate the existence of a logarithmic singularity, one needs to take a partial derivative with respect to  $\lambda$  on the determinant and sets  $\lambda$  as the previous solution ( $\lambda_0$ ) to assume a power function distribution. If  $\frac{\partial \text{Det}}{\partial \lambda} = 0$  ( $\lambda = \lambda_0$ ), then there exists the logarithmic singularities, which will not be repeated below. For general cases, readers can refer to the Supplemental Materials for scripts and conduct specific case studies.

# 4.4. Singularity caused by interfacial materials at $\beta \rightarrow 0$

When a structure exhibits deficits or cracks, a rapid and economical repair method is to clean the cracks and fill adhesive materials for lifetime extension and safety enhancement. In this case,  $\beta \to 0$  is considered. Although the volume of adhesive material approaches zero, the stiffness of the adhesive plays a significant role in the stress singularity and discontinuity. The present method based on the Eshelby's EIM provides a unique way to investigate this problem. Given an angle  $\beta$ , the singularity parameter  $\lambda$  depends on the material mismatch described by Dundurs' parameters (Dundurs, 1969) as follows:

$$\overline{\alpha} = \frac{\gamma(k_0 + 1) - (k_1 + 1)}{\gamma(k_0 + 1) + (k_1 + 1)}; \quad \overline{\beta} = \frac{\gamma(k_0 - 1) - (k_1 - 1)}{\gamma(k_0 + 1) + (k_1 + 1)}$$

$$(60)$$

where  $\overline{\alpha}$  and  $\overline{\beta}$  are equivalent to Dundurs' work and  $\overline{(.)}$  differentiates it from angles used in this paper;  $\gamma = \mu^0/\mu^1$  and  $k_i = 3 - 4v_i$  (i = 0, 1). Given elastic constants of the inhomogeneity and matrix,  $\overline{\alpha}$  and  $\overline{\beta}$  are key parameters determining the singularity parameter  $\lambda$ . For instance, given Poisson's ratios of two materials, the singularity should depend on  $\overline{\alpha}$  and  $\overline{\beta}$ , which can be verified by adjusting shear modulus proportionally. When  $\beta \to 0$ , the numerical results can be directly applied to adhesive interfaces in layered materials or laminated composite.

According to Dundur's results,  $\overline{\alpha}$  and  $\overline{\beta}$  are limited in a parallelogram region, where  $\overline{\alpha} \in [-1, 1]$  and  $\overline{\beta} \in [-0.5, 0.5]$ , respectively, with some pairs of  $(\overline{\alpha}, \overline{\beta})$  not physical. To investigate the effects of elastic constants, 21 uniform points of  $\overline{\alpha}$  and  $\overline{\beta}$  are selected.

Table 1 and Table 2 show singularity order of Mode I and Mode II, respectively. Indicated as Table 1, when  $\bar{\alpha} = -1$ ,  $\lambda = 0.5$  for all cases. In Fig. 2 of Dundurs (1969),  $\bar{\alpha} = -1$  is the left border of the parallelogram, and  $\gamma = 0$  implies the maximum material mismatch. In such a case, the change of Poisson's ratio does influence the singularity order. And such situations can be observed in Table 2 as well.

When  $\overline{\alpha}$  gradually increases, say 0.9,0.8 for example,  $\lambda$  decreases rapidly from 0.5 to less than 0.1. A similar phenomenon can be observed in Fig. 5(a), suggesting that increasing stiffness of inhomogeneity can efficiently reduce singular effects. For the same  $\overline{\alpha} \in [-1,0)$ ,  $\lambda$  decreases with larger  $\overline{\rho}$ , which can be interpreted as narrowing material mismatch. It can be observed that when  $\overline{\alpha} = 0$ , stress singularity disappears for all cases of  $\overline{\rho}$ . When  $\overline{\alpha} \in (0,1]$ , singularity starts to appear again and the number of points (singularity) gradually increases.

A special case with logarithmic singularity  $(\overline{\alpha}, \overline{\beta}) = (0.3, -0.15)$  is annotated with (\*), as the partial derivative of the determinant also yields as zero with the same  $\lambda$ . As an inverse trend of  $\overline{\alpha} \in [-0.1,0)$ ,  $\lambda$  increases with  $\overline{\alpha}$ , which can also be attributed as greater material mismatch. Finally, when  $overline\alpha$  equals 1,  $\gamma \to \infty$  and  $\lambda$  become 0.5 again for maximum material mismatch. Similarly, the solution does not change with variation of Poisson's ratios.

Table 2 displays singularity parameters of mode II versus  $\overline{\alpha}$  and  $\overline{\beta}$ . Similar to Table 1, with narrowing material mismatch,  $\lambda$  rapidly decreases, such as from 0.5 to less than 0.02. The singularity does not always exist for constant  $\overline{\alpha}$ . It can be observed that when  $\overline{\alpha} \in [0.1, 0.9]$ , there exist no singularities for mode II. And when  $\overline{\alpha} = 1$ ,  $\lambda$  become 0.5 for the maximum material mismatch, which does not vary with Poisson's ratios.

Note that the logarithmic singularity in the inhomogeneity problem with  $\mu_1/\mu_0 \neq 0$  can be significantly different from the wedge problem due to the boundary conditions (Bogy, 1968; Dempsey and Sinclair, 1979). This paper demonstrates the singularity along the line of  $x_2 = 0$  or  $\theta = 0$  only, the singularity along other lines across the origin (0,0) can also be derived in the similar fashion. The cases for  $\beta = \frac{\pi}{12}, \frac{\pi}{6}, \frac{\pi}{4}, \frac{\pi}{3}$  are provided in Supplementary Materials.

## 5. Remarks about the significant results and future extensions

This paper extended Eshelby's equivalent inclusion method (EIM) (Eshelby, 1956) to angular inhomogeneity, which exhibits complex singularity depending on the stiffness mismatch, opening angle, and loading conditions. Some remarks are provided about the significance of this work and its future extensions as follows:

- 1. Although this work used Eshelby's EIM (Eshelby, 1956) to investigate the singularity of the angular inhomogeneity, while Rodin (1996) already solved the corresponding inclusion problem, we cannot reproduce Eshelby's solution of the ellipsoidal inhomogeneity problem in the present angular inhomogeneity problem based on Rodin's solution, as a singular eigenstrain is expected. To our knowledge, this is the first work to study elastic field caused by a singular eigenstrain field with an analytical solution, although uniform and polynomial eigenstrain fields have been addressed well in the literature (Mura, 1987; Yin et al., 2007; Wu and Yin, 2021; Wu et al., 2021).
- 2. Mathematically, the problem of the singularity in an angular inhomogeneity is reduced to search the eigenstrain with singularity parameter  $\lambda$  to generate a stress field at the same singularity order around the vertex by applying the stress equivalent condition. Different inhomogeneity shape, stiffness ratio, and loading conditions lead to different  $\lambda$ .
- 3. Although the stress discontinuity along the boundary of an inclusion or inhomogeneity has been studied for ellipsoidal particles (Mura, 1987; Ju and Sun, 1999), it is the first time for this paper to show the exact solution in Eq. (7) for the stress jump cross the interface for polygonal inclusions with the explicit integral, which should credit to Rodin's original work (Rodin, 1996) although he did not provide the formulation yet. This analytical form of the discontinuity assures the exactness and rigorousness of the analysis for singularity.
- 4. Although the singularity of slit-like cracks or wedge problems has been well studied (Williams, 1956; Dempsey and Sinclair, 1981; Mura, 1987), angular inhomogeneity problems are commonly solved by numerical methods only, and this is the first work analytically investigating the singularity at the vertex of an angular inhomogeneity. Although we used the wedge or open cracking problems existing in the literature to verify the solution in special cases, this is the first analytical solution of the singularities of general inhomogeneities embedded in a matrix that exhibit different boundary conditions from the wedge problems. This method is versatile. It not only verifies a spectrum of existing solutions, but also discovers singularity parameters for general inhomogeneities.
- 5. For a polygonal inhomogeneity in a matrix, the singularity on each vertex depends on its opening angle, which can be used in material design to control stress singularity. Moreover, the present method can provide the singular eigenstrain field around the vertex in superposition of continuously distributed eigenstrain in the domain, which can expedite simulation of polygonal inhomogeneities with much less effort in particle discretization (Wu et al., 2021). The understanding of stress singularity can further serve as a guidance for other numerical interpolations, such as extended-FEM (Fries and Belytschko, 2010).
- 6. When a polyhedral inhomogeneity is embedded in a matrix, the singularity in the neighborhood of the edge and vertex is another challenging problem in the solid mechanics. Although the Airy's stress function cannot be directly used in 3D problems, the concept of this paper can be extended to 3D cases by using the singular eigenstrain with Eshelby's EIM. Particularly, the singularity along the edge can be straightforwardly predicted by the 2D solution, while the singularity around the vertex is subjected to a higher order of singularity depending on the sharpness of the angle, stiffness ratio, and loading condition, which is open for future studies.

)     	-0.5	-0.45	-0.4	-0.35	-0.3	-0.25	-0.2	-0.15	-0.1	-0.05	0	0.05	0.1	0.15	0.2	0.25	0.3	0.35	9.4	0.45	0.5
7	0.5	0.5	0.5	0.5	0.5	0.5	0.5	0.5	0.5	0.5	0.5	N/A	N/A	N/A	N/A	N/A	N/A	N/A	N/A	N/A	N/A
-0.9	N/A	0.0093	0.0091	0.0087	0.0081	0.0073	0.0063	0.0050	0.0036	0.0019	N/A	N/A	N/A	N/A	N/A	N/A	N/A	N/A	N/A	N/A	N/A
-0.8	N/A	N/A	0.0043	0.0042	0.0039	0.0035	0.0031	0.0025	0.0018	0.00094	N/A	N/A	N/A	N/A	N/A	N/A	N/A	N/A	N/A	N/A	N/A
-0.7	N/A	N/A	0.00261	0.00258	0.00246	0.00226	0.00197	0.00161	0.00116	0.000621	N/A	N/A	N/A	N/A	N/A	N/A	N/A	N/A	N/A	N/A	N/A
-0.6	N/A	N/A	0.00101	0.00114	0.00118	0.00115	0.00105	0.000887	0.000657	0.000363	N/A	N/A	N/A	N/A	N/A	N/A	N/A	N/A	N/A	N/A	N/A
-0.5	N/A	N/A	N/A	N/A	0.000755	0.00081	0.000782	0.000685	0.000522	0.000295	N/A	N/A	N/A	N/A	N/A	N/A	N/A	N/A	N/A	N/A	N/A
-0.4	N/A	N/A	N/A	N/A	N/A	0.000447	0.00053	0.000511	0.000412	0.000243	N/A	N/A	N/A	N/A	N/A	N/A	N/A	N/A	N/A	N/A	N/A
-0.3	N/A	N/A	N/A	N/A	N/A	N/A	N/A	0.000305	0.000302	0.000197	N/A	N/A	N/A	N/A	N/A	N/A	N/A	N/A	N/A	N/A	N/A
-0.2	N/A	N/A	N/A	N/A	N/A	N/A	N/A	0.000305	0.000302	0.000197	N/A	N/A	N/A	N/A	N/A	N/A	N/A	N/A	N/A	N/A	N/A
-0.1	N/A	N/A	N/A	N/A	N/A	N/A	N/A	N/A	N/A	0.000136	N/A	N/A	N/A	N/A	N/A	N/A	N/A	N/A	N/A	N/A	N/A
0	N/A	N/A	N/A	N/A	N/A	N/A	N/A	N/A	N/A	N/A	N/A	N/A	N/A	N/A	N/A	N/A	N/A	N/A	N/A	N/A	N/A
0.1	N/A	N/A	N/A	N/A	N/A	N/A	N/A	N/A	N/A	0.0004	0.000444	0.000356	N/A	N/A	N/A	N/A	N/A	N/A	N/A	N/A	N/A
0.2	N/A	N/A	N/A	N/A	N/A	N/A	N/A	N/A	N/A	0.000227	0.000999	0.000944	0.000793	0.000542	N/A	N/A	N/A	N/A	N/A	N/A	N/A
0.3	N/A	N/A	N/A	N/A	N/A	N/A	N/A	0.0012*	0.000485	0.000185	0.00171	0.00167	0.00154	0.00135	0.00107	0.000706	N/A	N/A	N/A	N/A	N/A
0.4	N/A	N/A	N/A	N/A	N/A	N/A	N/A	N/A	0.000385	0.000163	0.00266	0.00262	0.00251	0.00232	0.00208	0.00176	0.00137	0.000878	N/A	N/A	N/A
0.5	N/A	N/A	N/A	N/A	N/A	N/A	N/A	N/A	0.000335	0.000148	0.00398	0.00394	0.00383	0.00365	0.0034	0.00309	0.0027	0.00225	N/A	N/A	N/A
9.0	N/A	N/A	N/A	N/A	N/A	N/A	N/A	N/A	N/A	0.000136	0.00596	0.00592	0.0058	0.00561	0.00534	0.005	0.00459	0.00411	0.00355	N/A	N/A
7:0	N/A	N/A	N/A	N/A	N/A	N/A	N/A	N/A	N/A	0.000127	0.00924	0.0092	0.00906	0.00884	0.00852	0.00813	0.00764	0.00708	0.00642	N/A	N/A
0.8	N/A	N/A	N/A	N/A	N/A	N/A	N/A	N/A	N/A	N/A	0.0158	0.0157	0.0155	0.0152	0.0148	0.0143	0.0136	0.0129	0.012	0.011	N/A
6.0	N/A	N/A	N/A	N/A	N/A	N/A	N/A	N/A	N/A	N/A	0.0346	0.0345	0.0342	0.0337	0.033	0.0321	0.0309	0.0296	0.0281	0.0264	N/A
-	N/A	N/A	N/A	N/A	N/A	N/A	N/A	N/A	N/A	N/A	0.5	0.5	0.5	0.5	0.5	0.5	0.5	0.5	0.5	0.5	0.5
																					ı

**Table 2** List of the singularity parameter  $\lambda$  of shearing loading case when  $\beta \to 0$ , versus two constants  $\overline{\alpha}$  and  $\overline{\beta}$ .

0.5	N/A	N/A	N/A	N/A	N/A	N/A	N/A	N/A	N/A	N/A	N/A	N/A	N/A	N/A	N/A	N/A	N/A	N/A	N/A	N/A	0.5
0.45	N/A	N/A	N/A	N/A	N/A	N/A	N/A	N/A	N/A	N/A	N/A	N/A	N/A	N/A	N/A	N/A	N/A	N/A	N/A	N/A	0.5
0.4	N/A	N/A	N/A	N/A	N/A	N/A	N/A	N/A	N/A	N/A	N/A	N/A	N/A	N/A	N/A	N/A	N/A	N/A	N/A	N/A	0.5
0.35	N/A	N/A	N/A	N/A	N/A	N/A	N/A	N/A	N/A	N/A	N/A	N/A	N/A	N/A	N/A	N/A	N/A	N/A	N/A	N/A	0.5
0.3	N/A	N/A	N/A	N/A	N/A	N/A	N/A	N/A	N/A	N/A	N/A	N/A	0.000333	N/A	0.5						
0.25	N/A	N/A	N/A	N/A	N/A	N/A	N/A	N/A	N/A	N/A	0.000999	0.000545	0.000167	N/A	0.5						
0.2	N/A	N/A	N/A	N/A	N/A	N/A	N/A	N/A	0.002	0.00133	0.000799	0.000363	N/A	N/A	N/A	N/A	N/A	N/A	N/A	N/A	0.5
0.15	N/A	N/A	N/A	N/A	0.00695	N/A	0.00365	0.00256	0.00175	0.00111	0.0006	0.000182	N/A	N/A	N/A	N/A	N/A	N/A	N/A	N/A	0.5
0.1	N/A	N/A	N/A	N/A	0.00646	0.00478	0.00332	0.00228	0.0015	0.000888	0.0004	N/A	N/A	N/A	N/A	N/A	N/A	N/A	N/A	N/A	0.5
0.05	N/A	N/A	0.0167	0.0099	0.00596	0.00438	0.00299	0.002	0.00125	0.000666	0.0002	N/A	N/A	N/A	N/A	N/A	N/A	N/A	N/A	N/A	0.5
0	0.5	0.0346	0.0157	0.00924	0.00547	0.00398	0.00266	0.00171	0.000999	0.000444	N/A	N/A	N/A	N/A	N/A	N/A	N/A	N/A	N/A	N/A	0.5
-0.05	0.5	0.0327	0.0148	0.00859	0.00497	0.00359	0.00233	0.00143	0.000749	0.000222	N/A	N/A	N/A	N/A	N/A	N/A	N/A	N/A	N/A	N/A	N/A
-0.1	0.5	0.0309	0.0138	0.00793	0.00448	0.00319	0.002	0.00114	0.0005	N/A	N/A	N/A	N/A	N/A	N/A	N/A	N/A	N/A	N/A	N/A	N/A
-0.15	0.5	0.029	0.0128	0.00728	0.00398	0.00279	0.00166	0.000856	0.00025	N/A	N/A	N/A	N/A	N/A	N/A	N/A	N/A	N/A	N/A	N/A	N/A
-0.2	0.5	0.0272	0.0118	0.00662	0.00349	0.00239	0.00133	0.000571	N/A	N/A	N/A	N/A	N/A	N/A	N/A	N/A	N/A	N/A	N/A	N/A	N/A
-0.25	0.5	0.0253	0.0109	0.00596	0.00299	0.002	0.000999	0.000286	N/A	N/A	N/A	N/A	N/A	N/A	N/A	N/A	N/A	N/A	N/A	N/A	N/A
-0.3	0.5	0.0234	0.0099	0.0053	0.00249	0.0016	0.000666	N/A	N/A	N/A	N/A	N/A	N/A	N/A	N/A	N/A	N/A	N/A	N/A	N/A	N/A
-0.35	0.5	0.0215	0.00892	0.00464	0.002	0.0012	0.000333	N/A	N/A	N/A	N/A	N/A	N/A	N/A	N/A	N/A	N/A	N/A	N/A	N/A	N/A
-0.4	0.5	0.0196	0.00793	0.00398	N/A	N/A	N/A	N/A	N/A	N/A	N/A	N/A	N/A	N/A	N/A	N/A	N/A	N/A	N/A	N/A	N/A
-0.45	0.5	0.0177	0.00695	N/A	N/A	N/A	N/A	N/A	N/A	N/A	N/A	N/A	N/A	N/A	N/A	N/A	N/A	N/A	N/A	N/A	N/A
-0.5	0.5	N/A	N/A	N/A	N/A	N/A	N/A	N/A	N/A	N/A	N/A	N/A	N/A	N/A	N/A	N/A	N/A	N/A	N/A	N/A	N/A
la	7	-0.9	-0.8	-0.7	-0.6	-0.5	-0.4	-0.3	-0.2	-0.1	0	0.1	0.2	0.3	9.4	0.5	9.0	0.7	0.8	6.0	1

The method can be extended to other multi-physical problems with angular inhomogeneities embedded into a matrix, such as electric, thermal, and magnetic problems. The singularity behavior of the thermoelastic problems (Wu et al., 2023) is shown in the Supplementary Materials. The extension from a 2D problem of polygonal inhomogeneities to a 3D problem of cone-shaped or polyhedral inhomogeneities is underway.

#### 6. Conclusions

The boundary value problem for a triangular inhomogeneity embedded in an unbounded matrix has been mathematically converted to integral equations by Eshelby's EIM. By applying Airy's stress function and asymptotic analysis, the domain integrals of second-order partial derivatives of Green's function with the eigenstrain can be expressed through distance and opening angle. The discontinuities of the Eshelby's tensor along the boundary and vertex of the inhomogeneity are analytically derived. The dominant singular term for elastic fields can be separated by the Taylor series expansion. The singular eigenstrain distribution around the vertex can be derived, which show the same singularity rank as exterior stress fields. The equivalent inclusion method has been extended to identify dominant singularities for general triangular voids which are verified with classic solutions. For triangular inhomogeneities, EIM compresses the number of equations as two for either symmetric or anti-symmetric problem without solving four equations in the conventional methods. By solving the eigenvalue problem of the coefficient matrix and its partial derivative with respect to the singularity parameter, this method can be easily extended to general inhomogeneities subjected to the two loading conditions with logarithmic singularity. With a systemically understanding of the eigenstrain around the vertex, the EIM-related numerical treatments on singularities become possible.

## CRediT authorship contribution statement

**Chunlin Wu:** Conceptualization, Data curation, Methodology, Validation, Visualization, Writing – original draft. **Huiming Yin:** Conceptualization, Funding acquisition, Writing – review & editing.

#### Declaration of competing interest

The authors of the manuscript declare that they do not have any competing interests or conflicts.

## Data availability

All data/model used in the manuscript is available in the supplementary information.

# Acknowledgments

This work is supported by the Chenguang Program of Shanghai Education Development Foundation and Shanghai Municipal Education Commission, China, National Science Foundation of China 12302086, National Science Foundation IIP, United States #1941244 and U.S. Department of Agriculture NIFA #2021-67021-34201, whose support is gratefully acknowledged.

## Appendix A. Components of eigenstrain, displacement gradients and Green's function in Cartesian coordinate

## A.1. Eigenstrain components in the Cartesian coordinate

A strain transformation can be applied to the eigenstrain in Eq. (22) from the polar coordinate to the Cartesian coordinate as follows:

$$\begin{split} \varepsilon_{11}^* &= \frac{\partial}{\partial \lambda} \left\{ \frac{(\lambda - 1)}{2\mu^0 \mu^1} r^{-\lambda} \left( c_1 (\lambda - 2) (\mu^0 - \mu^1) \sin \lambda \theta - c_2 (\lambda - 2) (\mu^0 - \mu^1) \cos \lambda \theta - 2 c_3 \mu^0 \sin \lambda \theta \right. \right. \\ &\quad - c_3 \lambda \mu^0 \sin(\lambda + 2) \theta - 2 c_4 \mu^0 \cos \lambda \theta - c_4 \lambda \mu^0 \cos(\lambda + 2) \theta + 2 c_3 \mu^1 \sin \lambda \theta \\ &\quad + c_3 \lambda \mu^1 \sin(\lambda + 2) \theta + 2 c_4 \mu^1 \cos \lambda \theta + c_4 \lambda \mu^1 \cos(\lambda + 2) \theta - 4 c_3 \mu^1 v^0 \sin \lambda \theta \\ &\quad - 4 c_4 \mu^1 v^0 \cos \lambda \theta + 4 c_3 \mu^0 v^1 \sin \lambda \theta + 4 c_4 \mu^0 v^1 \cos \lambda \theta \right) \right\} \\ \varepsilon_{12}^* &= -\frac{\partial}{\partial \lambda} \left\{ \frac{(\lambda - 1)(\mu^0 - \mu^1)}{2\mu^0 \mu^1} r^{-\lambda} \left( c_2 (\lambda - 2) \sin \lambda \theta + c_4 \lambda \sin(\lambda + 2) \theta + c_1 (\lambda - 2) \cos \lambda \theta - c_3 \lambda \cos(\lambda + 2) \theta \right) \right\} \\ \varepsilon_{22}^* &= -\frac{\partial}{\partial \lambda} \left\{ \frac{(\lambda - 1)}{2\mu^0 \mu^1} r^{-\lambda} \left( c_1 (\lambda - 2)(\mu^0 - \mu^1) \sin \lambda \theta - c_2 (\lambda - 2)(\mu^0 - \mu^1) \cos \lambda \theta + 2 c_3 \mu^0 \sin \lambda \theta \right. \\ &\quad - c_3 \lambda \mu^0 \sin(\lambda + 2) \theta + 2 c_4 \mu^0 \cos \lambda \theta - c_4 \lambda \mu^0 \cos(\lambda + 2) \theta - 2 c_3 \mu^1 \sin \lambda \theta \right. \\ &\quad + c_3 \lambda \mu^1 \sin(\lambda + 2) \theta - 2 c_4 \mu^1 \cos \lambda \theta + c_4 \lambda \mu^1 \cos(\lambda + 2) \theta + 4 c_3 \mu^1 v^0 \sin \lambda \theta \right. \\ &\quad + 4 c_4 \mu^1 v^0 \cos \lambda \theta - 4 c_3 \mu^0 v^1 \sin \lambda \theta - 4 c_4 \mu^0 v^1 \cos \lambda \theta \right) \right\} \end{split}$$

## A.2. Displacement gradients in the Cartesian coordinate

$$\begin{aligned} u_{1,2} &= -\frac{\partial}{\partial \lambda} \left\{ \begin{array}{l} \frac{(\lambda-1)r^{-2-\lambda}}{2\mu^1} \left( c_3 \left[ -\left(x_1^2(\lambda-4v^1+4)\cos\lambda\theta\right) + x_2^2(\lambda+4v^1-4)\cos\lambda\theta + 2\lambda x_1 x_2\sin\lambda\theta \right] \right. \\ &+ c_1(\lambda-2)r^2\cos\lambda\theta \left. \right) \right\} \\ u_{2,1} &= -\frac{\partial}{\partial \lambda} \left\{ \begin{array}{l} \frac{(\lambda-1)r^{-2-\lambda}}{2\mu^1} \left( c_3 \left[ -\left(x_1^2(\lambda+4v^1-4)\cos\lambda\theta\right) + x_2^2(\lambda-4v^1+4)\cos\lambda\theta + 2\lambda x_1 x_2\sin\lambda\theta \right] \right. \\ &+ c_1(\lambda-2)r^2\cos\lambda\theta \left. \right) \right\} \end{aligned} \tag{A.2} \end{aligned}$$

## A.3. Derivatives of harmonic and biharmonic potentials

The Green's function is composed of biharmonic  $\psi$  and harmonic  $\phi$  potential functions, and some of their partial derivatives are listed below when the observing point is along the symmetric line  $\mathbf{x} = (x_1, 0)$ .

Biharmonic potential function

$$\psi_{,1111} = \frac{2\left(-r^4(\cos(4\theta) - 2\cos 2\theta) + 4r^3x_1\cos\theta(\cos 2\theta - 2) + 6r^2x_1^2 - 4rx_1^3\cos\theta + x_1^4\right)}{\left(r^2 - 2rx_1\cos\theta + x_1^2\right)^3}$$

$$\psi_{,1112} = -\frac{4r\sin\theta\left(r\cos\theta - x_1\right)\left(r^2(2\cos 2\theta - 1) - 2rx_1\cos\theta + x_1^2\right)}{\left(r^2 - 2rx_1\cos\theta + x_1^2\right)^3}$$

$$\psi_{,1122} = \frac{2\left(r^4\cos(4\theta) - 4r^3x_1\cos(3\theta) + 6r^2x_1^2\cos 2\theta - 4rx_1^3\cos\theta + x_1^4\right)}{\left(r^2 - 2rx_1\cos\theta + x_1^2\right)^3}$$

$$\psi_{,1212} = -\frac{r^4\cos(4\theta) - 4r^3x_1\cos(3\theta) + 6r^2x_1^2\cos 2\theta - 4rx_1^3\cos\theta + x_1^4}{2\pi(v - 1)\left(r^2 - 2rx_1\cos\theta + x_1^2\right)^3}$$

$$\psi_{,2212} = \frac{4r\sin\theta\left(r\cos\theta - x_1\right)\left(r^2(2\cos 2\theta + 1) + 3x_1\left(x_1 - 2r\cos\theta\right)\right)}{\left(r^2 - 2rx_1\cos\theta + x_1^2\right)^3}$$

$$\psi_{,2222} = \frac{6x_1\left(r^3\sin(4\theta)\csc\theta - x_1\left(2r^2(2\cos 2\theta + 1) - 4rx_1\cos\theta + x_1^2\right)\right) - 2r^4(2\cos 2\theta + \cos 4\theta)}{\left(r^2 - 2rx_1\cos\theta + x_1^2\right)^3}$$

Harmonic potential function

$$\phi_{,11} = \frac{2\left(r^2\cos 2\theta - 2rx_1\cos \theta + x_1^2\right)}{\left(r^2 - 2rx_1\cos \theta + x_1^2\right)^2}$$

$$\phi_{,12} = \frac{4r\sin \theta \left(r\cos \theta - x_1\right)}{\left(r^2 - 2rx_1\cos \theta + x_1^2\right)^2}$$

$$\phi_{,22} = -\frac{2\left(r^2\cos 2\theta - 2rx_1\cos \theta + x_1^2\right)}{\left(r^2 - 2rx_1\cos \theta + x_1^2\right)^2}$$
(A.4)

# Appendix B. Domain integrals of Green's function and eigenstrain under symmetric loading

This section provides domain integrals for step (iii) in Section 3.3 under symmetric loading, including  $\phi_{,11}\epsilon_{22}^*$ ,  $2\phi_{,12}\epsilon_{12}^*$ ,  $\cdots$ ,  $\psi_{,2222}\epsilon_{22}^*$ .

$$\begin{split} &\int_{\varOmega^p} \phi_{,11} H_{22}(\lambda,\beta) r^{-\lambda} d\mathbf{x}' = |x_1|^{-\lambda} \frac{\pi(\lambda-1)}{8\mu^0\mu^1} \left\{ 2c_4 \csc \lambda \pi \left[ (\lambda-1) \left[ 2(\mu^0-\mu^1) \sin \lambda(\pi-2\beta) - \lambda(\mu^0-\mu^1) \sin(\lambda\pi+4\beta) \right. \right. \right. \\ &\left. + 4 \left( \sin(\lambda\pi+2\beta) - \sin[\lambda\pi+2\beta(1-\lambda)] \right) \left[ \mu^0 (1-2v^1) - \mu^1 (1-2v^0) \right] \right] + (\lambda-2) \sin \lambda \pi \left[ \mu^0 (\lambda+8v^1-5) - \mu^1 (\lambda+8v^0-5) \right] \right] \\ &\left. - 4c_2 (\lambda-2)(\mu^0-\mu^1) \left[ \csc \lambda \pi \left( (\lambda-1) \sin(\lambda\pi+2\beta) - \sin[\lambda\pi+2\beta(1-\lambda)] \right) - \lambda + 2 \right] \right\} \\ &\int_{\varOmega^p} \phi_{,12} H_{12}(\lambda,\beta) r^{-\lambda} d\mathbf{x}' = -|x_1|^{-\lambda} \frac{\pi(\lambda-1) \csc \lambda \pi (\mu^0-\mu^1)}{4\mu^0\mu^1} \left\{ c_4 (\lambda-1) \left[ 2 \sin \lambda(\pi-2\beta) + \lambda \sin(\lambda\pi+4\beta) \right. \right. \\ &\left. - \left[ (\lambda+2) \sin \lambda\pi \right] \right] + 4c_2 (\lambda-2) \left[ \lambda \sin \beta \cos(\lambda\pi+\beta) - \sin \lambda\beta \cos[\lambda\pi+\beta(2-\lambda)] \right] \right\} \\ &\int_{\varOmega^p} \phi_{,22} H_{11}(\lambda,\beta) r^{-\lambda} d\mathbf{x}' = |x_1|^{-\lambda} \frac{\pi(1-\lambda) \csc \lambda\pi}{4\mu^0\mu^1} \left\{ c_4 (\lambda-1)(\mu^0-\mu^1) \left[ \lambda \sin(\lambda\pi+4\beta) - 2 \sin \lambda(\pi-2\beta) \right] \right. \\ &\left. + 2 \left[ (\lambda-1) \sin(\lambda\pi+2\beta) - \sin[\lambda\pi+2\beta(1-\lambda)] \right] \left[ c_2 (\lambda-2)(\mu-\mu^1) + 2c_4 \left[ \mu^0 (1-2v^1) - \mu^1 (1-2v^0) \right] \right] \end{aligned} \tag{B.3} \\ &\left. + (2-\lambda) \sin \lambda\pi \left[ 2c_2 (\lambda-2)(\mu-\mu^1) + c_4 \left[ \mu^1 (-\lambda+8v^0-3) + \mu(\lambda-8v^1+3) \right] \right] \right\} \end{split}$$

$$\int_{\Omega^{p}} w_{1,112} H_{11}(\lambda, \beta) p^{-\lambda} dx' = |x_{1}|^{-\lambda} \frac{\pi(\lambda - 1)}{24\mu^{0}\mu^{\lambda}} \left\{ \cos(\lambda - 2) \cos(\lambda \pi(\mu^{0} - \mu^{1}) \left[ (\lambda - 4)(\lambda - 1) \sin(\lambda \pi + 2\beta) - (\lambda - 4) \sin(\lambda \pi + 2\beta) - ($$

## Appendix C. Domain integrals of Green's function and eigenstrain under anti-symmetric loading

This appendix aims to provide supplementary information on domain integrals (step (iii)) from Section 3.3 under anti-symmetric loading. Because disturbed shear strain has more compact expressions, this section compresses contribution from  $\phi$  and eigenstrain into two short equations; and domain integrals of  $\psi_{,1211}\varepsilon_{11}^*$ ,  $\psi_{12,22}\varepsilon_{22}^*$  and  $2\psi_{,1212}\varepsilon_{12}^*$  are provided.

(i) Contribution by  $\phi$  and eigenstrain for the first equation of the shearing case:

$$\begin{split} &\frac{1}{8\pi(1-v^0)}\int_{\Omega^p} -2v^0\phi_{,12}\big[H_{11}(\lambda,\beta)+H_{22}(\lambda,\beta)\big] -2(1-v^0)\big[H_{12}(\lambda,\beta)(\phi_{,11}+\phi_{,22})+\phi_{,12}\big(H_{11}(\lambda,\beta)+H_{22}(\lambda,\beta)\big)\big]r^{-\lambda}d\mathbf{x}'\\ &=|x_1|^{-\lambda}\frac{c_3}{\mu^0\mu^1(1-v^0)}(\lambda-1)\csc\lambda\pi\Big[\lambda\sin\beta\cos[\lambda\pi+\beta]-\sin\lambda\beta\cos[\lambda\pi+(2-\lambda)\beta]\Big]\Big[\mu^0(1-2v^1)-\mu^1(1-2v^0)\Big] \end{split} \tag{C.1}$$

(ii) Contribution by  $\phi$  and eigenstrain for the second equation of the shearing case:

$$\begin{split} &\frac{1}{8\pi(1-v^0)}\int_{\Omega^p}-2v^0\phi_{,12}\big[H_{11}(\lambda,\beta)+H_{22}(\lambda,\beta)\big]-4(1-v^0)\big[\phi_{,11}H_{11}(\lambda,\beta)+\phi_{,12}H_{12}(\lambda,\beta)\big]r^{-\lambda}d\mathbf{x}'\\ &=-|x_1|^{-\lambda}\frac{(\lambda-1)\csc\lambda\pi}{4\mu^0\mu^1(1-v^0)}\left\{-4c_1(\lambda-2)(1-v^0)(\mu^0-\mu^1)\sin(1-\lambda)\beta\cos[\lambda\pi+\beta(1-\lambda)]\\ &+2c_3\left[(\lambda-1)(1-v^0)(\mu^0-\mu^1)\sin\lambda(\pi-2\beta)-\left[(\lambda-1)\sin(\lambda\pi+2\beta)+\sin[\lambda\pi+2\beta(1-\lambda)]\right]\left[\mu^0(1-2v^1)-\mu^1(1-2v^0)\right]\\ &+\sin\lambda\pi\left[\mu^0(\lambda v^0-2\lambda v^1-v^0+1)+\mu^1(\lambda v^0+v^0-1)\right]\right]\right\} \end{split}$$

(iii)  $\psi_{,1211} \varepsilon_{11}^*$ 

$$\begin{split} &\frac{1}{8\pi(1-v^0)}\int_{\varOmega^p}\psi_{,1211}H_{11}(\lambda,\beta)r^{-\lambda}d\mathbf{x}'\\ &=-|x_1|^{-\lambda}\frac{(\lambda-1)}{384\mu^0\mu^1(1-v^0)}\left\{\begin{array}{l}\csc\lambda\pi\left[\begin{array}{l}c_3\left[\begin{array}{l}-12(\lambda-2)(\lambda-1)(\mu^0-\mu^1)\sin\lambda(\pi-2\beta)+4(\lambda-2)(\lambda-1)\lambda(\mu^0-\mu^1)\right.\\ &\sin(\lambda\pi+6\beta)-24(\lambda-2)(\lambda-1)\sin(\lambda\pi+2\beta)\left[\mu^0(1-2v^1)-\mu^1(1-2v^0)\right]-6(\lambda-2)(\lambda-1)\sin(\lambda\pi+4\beta)\\ &\left(\mu^0(\lambda+4v^1-2)-\mu^1(\lambda+4v^0-2)\right)+12(\lambda-2)\sin[\lambda\pi+2\beta(1-\lambda)]\left[\mu^0(\lambda+4v^1-2)-\mu^1(\lambda+4v^0-2)\right]\\ &+24(\lambda-1)\sin[\lambda\pi+2\beta(2-\lambda)]\left[\mu^0(1-2v^1)-\mu^1(1-2v^0)\right]\right]-3c_1(\lambda-2)(\mu^0-\mu^1)\left[\begin{array}{l}2(\lambda-2)\left(\begin{array}{l}(\lambda-1)\left[\sin(\lambda\pi+4\beta)(\lambda-2)(\mu^0-\mu^1)\right]\\ -2\sin(\lambda\pi+2\beta)\end{array}\right]\\ &-2\sin(\lambda\pi+2\beta)\end{array}\right]-2\sin(-2\beta\lambda+2\beta+\pi\lambda)\left(\frac{1}{2}+4\lambda^2+1\right)+4\lambda^2(\lambda-1)\sin(-2\beta\lambda+4\beta+\pi\lambda)\right)\right]\\ &+c_3(4\mu^0-4\mu^1+\lambda\mu^1(\lambda-12v^0+6)-\lambda\mu^0(\lambda-12v^1+6))\end{array}\right] \end{split}$$

(iv)  $\psi_{.1212}\varepsilon_{12}^*$ 

$$\begin{split} &\frac{1}{8\pi(1-v^0)}\int_{\Omega^p}\psi_{,1212}H_{12}(\lambda,\beta)r^{-\lambda}d\mathbf{x}'\\ &=-|x_1|^{-\lambda}\frac{(\lambda-1)(\mu^0-\mu^1)}{384\mu^0\mu^1(1-v^0)}\left\{\ 2(\lambda-2)\left[3c_1\left(\lambda^2+\lambda-4\right)-c_3\lambda(\lambda+5)\right]-\csc\lambda\pi\left[\ 12c_3\lambda\left[\ (\lambda-1)\sin((\pi-2\beta)\lambda)\right.\right.\right.\\ &\left.-(\lambda-2)\sin[\lambda\pi+2\beta(1-\lambda)]+\lambda(\lambda-2)(\lambda-1)^2\left(\cos[2\lambda\pi+10\beta]-\cos2\beta\right)\right]-3c_1(\lambda-2)\left[\ 2(\lambda-1)\left(\ (\lambda-2)\sin(\lambda\pi+4\beta)\right.\right.\right.\\ &\left.-2\lambda\sin(\lambda\pi+2\beta)\right)+4\sin[\lambda\pi+2\beta(2-\lambda)]-8\lambda\sin\beta\cos[\lambda\pi+(3-2\lambda)\beta]\left.\right]\right\} \end{split}$$

 $\psi_{,1222}\varepsilon_{22}^*$ 

$$\begin{split} &\frac{1}{8\pi(1-v^0)}\int_{\Omega^p}\psi_{,1222}H_{22}(\lambda,\beta)r^{-\lambda}d\mathbf{x}'\\ &=-|x_1|^{-\lambda}\frac{(\lambda-1)}{384\mu^0\mu^1(1-v^0)}\left\{-\csc\lambda\pi\left[c_3\left[12\left(\lambda^2+\lambda-2\right)(\mu^0-\mu^1)\sin\lambda(\pi-2\beta)-4(\lambda-2)(\lambda-1)\lambda(\mu^0-\mu^1)\right]\right.\\ &\sin(\lambda\pi+6\beta)-24\left[\lambda^2+\lambda-2\right]\sin(\lambda\pi+2\beta)\left[\mu^0(1-2v^1)-\mu^1(1-2v^0)\right]+12\sin[\lambda\pi+2\beta(1-\lambda)]\left[\mu^1\left(\lambda^2-4(\lambda+2)v^0+4\right)+\mu^0\left(-\lambda^2+4(\lambda+2)v^1-4\right)\right]+6(\lambda-1)\sin(\lambda\pi+4\beta)\left[\mu^1(-\lambda(\lambda+4)+4(\lambda-2)v^0+4)+\mu^1(\lambda(\lambda+4)-4(\lambda-2)v^1-4)\right]\\ &+24(\lambda-1)\sin[\lambda\pi+2\beta(2-\lambda)]\left[\mu^0(1-2v^1)-\mu^1(1-2v^0)\right]-3c_1(\lambda-2)(\mu^0-\mu^1)\left(4\left[\lambda^2+\lambda-2\right]\sin(\lambda\pi+2\beta)\\ &-2(\lambda-2)(\lambda-1)\sin(\lambda\pi+4\beta)+4(\lambda+2)\sin(-2\beta\lambda+2\beta+\pi\lambda)-4(\lambda-1)\sin[\lambda\pi+2\beta(2-\lambda)]\right)\right]\\ &-2\left[3c_1(\lambda-2)\lambda(\lambda+5)(\mu^0-\mu^1)+c_3(12\mu^0-12\mu^1+\lambda\mu^1\left[\lambda(\lambda+3)+12(\lambda+5)v^0-22\right]-\lambda\mu^0\left[\lambda(\lambda+3)+12(\lambda+5)v^1-22\right)\right]\right]\right\} \end{split} \tag{C.5}$$

## Appendix D. Supplementary data

Supplementary material related to this article can be found online at https://doi.org/10.1016/j.jmps.2024.105545. The following information has been included in the Supplementary Materials: (1) the Mathematics scripts for the long equations; (2) the singularity caused by an angular inhomogeneity with different opening angles, and; (3) the extension of this method to thermoelastic problems.

#### References

Aliabadi, M.H., 2002. The Boundary Element Method Vol2: Applications in Solids and Structures. Vol. 2, Wiley.

Barber, J.R., 1992. Elasticity. Springer Dordrecht, Dordrecht.

Bogy, David B., 1968. Edge-bonded dissimilar orthogonal elastic wedges under normal and shear loading. J. Appl. Mech. 35 (3), 460-466.

Boussinesq, Joseph, 1885. Applications Des Potentiels. Vol. 4, Gauthier-Villars.

Bulatov, Vasily, Cai, Wei, 2006. Computer Simulations of Dislocations. OUP, Oxford.

Chiang, Chun-Ron, 2015. Problems of polygonal inclusions in orthotropic materials with due consideration on the stresses at corners. Arch. Appl. Mech. 86 (5),

Dempsey, J.P., Sinclair, G.B., 1979. On the stress singularities in the plane elasticity of the composite wedge. J. Elasticity 9 (4), 373-391.

Dempsey, J.P., Sinclair, G.B., 1981. On the singular behavior at the vertex of a bi-material wedge. J. Elasticity 11 (3), 317-327

Dundurs, J., 1969. Discussion: "Edge-bonded dissimilar orthogonal elastic wedges under normal and shear loading" (Bogy, DB, 1968, ASME J. Appl. Mech., 35, pp. 460-466). J. Appl. Mech..

Dundurs, John, Markenscoff, Xanthippi, 1989. A green's function formulation of anticracks and their interaction with load-induced singularities. J. Appl. Mech. 56 (3), 550-555.

Eshelby, J.D., 1951. The force on an elastic singularity. Philos. Trans. R. Soc. Lond. Ser. A Math. Phys. Sci. 244 (877), 87–112. Eshelby, J.D., 1956. The continuum theory of lattice defects. In: Solid State Physics. Elsevier, pp. 79–144.

Fries, Thomas-Peter, Belytschko, Ted, 2010. The extended/generalized finite element method: an overview of the method and its applications. Internat. J. Numer. Methods Engrg. 84 (3), 253-304.

Gao, X.-L., Liu, M.Q., 2012. Strain gradient solution for the Eshelby-type polyhedral inclusion problem. J. Mech. Phys. Solids 60 (2), 261-276.

Giordano, Stefano, Colombo, Luciano, 2007. Local elastic fields around cracks and their stress density of states. Phys. Rev. B 76 (17), 174120. Ju, J.W., Sun, L.Z., 1999. A novel formulation for the exterior-point eshelby's tensor of an ellipsoidal inclusion. J. Appl. Mech. 66 (2), 570–574.

Kröner, E., 1990. Modified green functions in the theory of heterogeneous and/or anisotropic linearly elastic media. In: Micromechanics and Inhomogeneity: The Toshio Mura 65th Anniversary Volume. Springer, pp. 197-211.

Ma, Lifeng, Korsunsky, Alexander M., 2014. The principle of equivalent eigenstrain for inhomogeneous inclusion problems. Int. J. Solids Struct. 51 (25-26), 4477-4484.

Martin, P.A., 1991. End-point behaviour of solutions to hypersingular integral equations. Proc.: Math. Phys. Sci. 432 (1885), 301-320.

Martin, P.A., 1992. Exact solution of a simple hypersingular integral equation. J. Integr. Equ. Appl. 4 (2), 197-204.

Mindlin, Raymond D., 1936. Force at a point in the interior of a semi-infinite solid. Physics 7 (5), 195-202.

Mura, Toshio, 1987. Micromechanics of Defects in Solids. Springer Netherlands.

Muskhelishvili, N.I., 2010. Some Basic Problems of the Mathematical Theory of Elasticity. Springer Netherlands.

Portela, A., Aliabadi, M.H., Rooke, D.P., 1993. Dual boundary element incremental analysis of crack propagation. Comput. Struct. 46 (2), 237-247.

Rice, J.R., 1968. A path independent integral and the approximate analysis of strain concentration by notches and cracks. J. Appl. Mech. 35 (2), 379-386.

Rodin, Gregory J., 1996. Eshelby's inclusion problem for polygons and polyhedra. J. Mech. Phys. Solids 44 (12), 1977-1995.

Ru, C.Q., 1999. Analytic solution for eshelby's problem of an inclusion of arbitrary shape in a plane or half-plane. J. Appl. Mech. 66 (2), 315-523.

Ru, C.Q., 2000. Eshelby's problem for two-dimensional piezoelectric inclusions of arbitrary shape. Proc. R. Soc. Lond. Ser. A Math. Phys. Eng. Sci. 456 (1997), 1051-1068

Sevostianov, Igor, Kachanov, Mark, 2007. Relations between compliances of inhomogeneities having the same shape but different elastic constants. Internat. J. Engrg. Sci. 45 (10), 797-806. Sun, L.G., Xu, K.Y., Pan, E., 2012. Inclusion of arbitrary polygon with graded eigenstrain in an anisotropic piezoelectric full plane. Int. J. Solids Struct. 49 (13),

1773-1785

Thomson (Lord Kelvin), William, 1848. Note on the integration of the equations of equilibrium of an elastic solid. Camb. Dublin Math. J. 3, 87-89.

Trotta, S., Marmo, F., Rosati, L., 2016. Analytical expression of the eshelby tensor for arbitrary polygonal inclusions in two-dimensional elasticity. Composites B 106, 48-58.

Trotta, S., Marmo, F., Rosati, L., 2017. Evaluation of the eshelby tensor for polygonal inclusions. Composites B 115, 170-181.

Wang, Min-Zhong, 1985. Application of the finite part of a divergent integral in the theory of elasticity. Appl. Math. Mech. 6.

Wang, Xu, Schiavone, Peter, 2021. New solutions for an Eshelby inclusion of arbitrary shape in a plane or two jointed half-planes. ZAMM - J. Appl. Math. Mech./Z. Angew. Math. Mech. 102 (1).

Williams, M.L., 1952. Stress singularities resulting from various boundary conditions in angular corners of plates in extension. J. Appl. Mech. 19 (4), 526-528. Williams, M.L., 1956. The complex-variable approach to stress singularities — II. J. Appl. Mech. 477-478.

Wu, Chunlin, Wang, Tengxiang, Yin, Huiming, 2023. The Green's function based thermoelastic analysis of a spherical geothermal tank in a semi-infinite domain. J. Mech. Phys. Solids 173, 105207.

Wu, Chunlin, Yin, H.M., 2021. Elastic solution of a polygon-shaped inclusion with a polynomial eigenstrain. J. Appl. Mech. 1-25.

Wu, Chunlin, Zhang, Liangliang, Yin, Huiming, 2021. Elastic solution of a polyhedral particle with a polynomial eigenstrain and particle discretization. J. Appl. Mech. 88 (12), 121001.

Yin, H.M., Paulino, G.H., Buttlar, W.G., Sun, L.Z., 2007. Micromechanics-based thermoelastic model for functionally graded particulate materials with particle interactions. J. Mech. Phys. Solids 55 (1), 132-160.

Yin, Huiming, Song, Gan, Zhang, Liangliang, Wu, Chunlin, 2022. The Inclusion-Based Boundary Element Method. IBEM, Academic Press.

Yin, H.M., Zhao, Yingtao, 2016. Introduction to the Micromechanics of Composite Materials. CRC PR INC.

Yuan, Tianyu, Liu, Liping, 2023. Polynomial inclusions: Definitions, applications, and open problems. J. Mech. Phys. Solids 181, 105440.

Yue, Y.M., Xu, K.Y., Chen, Q.D., Pan, E., 2015. Eshelby problem of an arbitrary polygonal inclusion in anisotropic piezoelectric media with quadratic eigenstrains. Acta Mech. 226 (7), 2365-2378.

Zhou, Kun, Hoh, Hsin Jen, Wang, Xu, Keer, Leon M., Pang, John H.L., Song, Bin, Wang, Q. Jane, 2013. A review of recent works on inclusions. Mech. Mater.

Zhou, Qinghua, Jin, Xiaoqing, Wang, Zhanjiang, Wang, Jiaxu, Keer, Leon M., Wang, Qian, 2014. Numerical implementation of the equivalent inclusion method for 2D arbitrarily shaped inhomogeneities. J. Elasticity 118 (1), 39-61. Zou, W.-N., He, Q.-C., 2017. Eshelby's problem of a spherical inclusion eccentrically embedded in a finite spherical body. Proc. R. Soc. A: Math. Phys. Eng. Sci.

473 (2198), 20160808. Zou, Wennan, He, Qichang, Huang, Mojia, Zheng, Quanshui, 2010. Eshelby's problem of non-elliptical inclusions. J. Mech. Phys. Solids 58 (3), 346–372.

Zou, W.-N., He, Q.-C., Zheng, Q.-S., 2012. Inclusions in a finite elastic body. Int. J. Solids Struct. 49 (13), 1627-1636.

Zou, Wen-Nan, Zheng, Quan-Shui, 2012. The second Eshelby problem and its solvability. Acta Mech. Sin. 28 (5), 1331.